

# Discrete Organic Nanotubes Based on a Combination of Covalent and Non-Covalent Approaches

Marco A. Balbo Block<sup>1</sup> · Christian Kaiser<sup>1</sup> · Anzar Khan<sup>1</sup> · Stefan Hecht<sup>1,2</sup> (✉)

<sup>1</sup> Institut für Chemie/Organische Chemie, Freie Universität Berlin, Takustr. 3, 14195 Berlin, Germany

*shecht@chemie.fu-berlin.de*

<sup>2</sup> Max-Planck-Institut für Kohlenforschung, Kaiser-Wilhelm-Platz 1, 45470 Mülheim an der Ruhr, Germany

*hecht@mpi-muelheim.mpg.de*

<b>1</b>	<b>Introduction</b>	90
<b>2</b>	<b>Tubular Design Principles</b>	92
<b>3</b>	<b>Tubes from Hollow Helical Backbones</b>	94
3.1	Inherently Stiff [ <i>n</i> ]Phenylene Helices	95
3.2	Helical Backbones Based on Intramolecular H-Bonding	96
3.2.1	Alternating D, L- $\alpha$ -Peptides	96
3.2.2	Aromatic and Heteroaromatic Amides	97
3.3	Helical Backbones Based on the <i>trans</i> -2,2'-Bipyridine Helicity Codon	101
3.3.1	Alternating Pyridine–Pyrimidine Oligomers	102
3.3.2	Alternating Pyridine–Pyridazine Oligomers	104
3.3.3	Alternating Naphthyridine–Pyrimidine Oligomers	105
3.4	Helical Backbones Based on Solvophobic Forces	105
3.5	Covalent Stabilization by Intramolecular Helical Crosslinking	110
<b>4</b>	<b>Tubes from Self-Assembled Helices and Sheets</b>	113
4.1	Multi-stranded Helices	113
4.2	Stacking Helices	114
4.3	Bundles	114
4.4	Barrels	115
<b>5</b>	<b>Tubes from Stacked Macrocycles</b>	117
5.1	Tubular Structures in the Solid State	117
5.1.1	Cyclic Peptides	117
5.1.2	Cyclic Oligosaccharides	120
5.1.3	Phenylene Macrocycles	121
5.1.4	Phenylene Ethynylene Macrocycles	121
5.2	Tubular Structures at Interfaces	125
5.3	Tubular Structures in Mesophases	125
5.4	Tubular Structures in Solution	126
5.4.1	Phenylene Ethynylene Macrocycles	126
5.4.2	Phenylene Diethynylene Macrocycles	126
5.4.3	Coil-Ring-Coil Block Copolymers	128
5.4.4	Covalent Stabilization by Crosslinking	129
5.4.5	Cyclodextrins	129
5.4.6	Cored Dendronized Polymers	130
5.4.7	Cyclic Alternating D, L- $\alpha$ -Peptides	130

6	<b>Tubes from Stacked Rosettes</b>	132
6.1	G-Quartets and Related Motifs	133
6.2	Melamine–Cyanuric Acid Motifs	135
7	<b>Tubes from Self-Assembled Amphiphiles</b>	138
7.1	Wedge-Shaped Amphiphiles	138
7.2	Linear Amphiphiles and Block Copolymers	140
8	<b>Conclusions and Outlook</b>	143
	<b>References</b>	145

**Abstract** Tubular organic nanostructures offering precise control over inner and outer surface functionality represent attractive building blocks for the bottom-up approach in nanotechnology, as well as for the development of future materials and biological applications. In this review, the current state of the art in creating organic nanotubes is summarized, focusing on the chemistry behind tubular structure formation. The discussion of general design principles, which are altogether inspired by Nature and combine covalent and non-covalent synthesis, is followed by detailed treatments of the individual approaches including helices and their assemblies, stacked rings and rosettes, as well as cylindrical micelles and rolled sheets. The authors provide a critical evaluation of past accomplishments, promising current developments, and future challenges in this fascinating and highly interdisciplinary research topic.

**Keywords** Materials science · Nanotubes · Self-assembly · Helices · Macrocycles

### Abbreviations

Aib	$\alpha$ -Aminoisobutyric acid
Cys(Acm)	Acetamidomethyl cysteine
Hag	Homoallylglycin
Htrp	Homotryptophane
N-MeAla	N-methyl alanine
RCM	Ring closing (olefin) metathesis
Triglyme	Tri(ethyleneglycol)
XR	X-ray specular reflectivity

## 1

### Introduction

Continuing miniaturization of electronic devices [1] represents the main driving force at the dawn of the nanotechnological era [2]. As established top-down methods, most notably photolithography, approach sub-100 nm resolution, emerging alternative bottom-up approaches based on the assembly of molecular building blocks promise to revolutionize nanofabrication [3]. In order to realize this ambitious goal, two major scientific challenges have to be mastered: (1) a molecular construction kit involving a diverse set of functional

units for generating, transporting, and converting signals is needed, in which the individual modules possess a certain shape and can be organized in a defined arrangement, preferably by self-assembly; and (2) the generated functional nanostructures have to be integrated into actual electronic devices, and therefore the connection to the macroscopic outside world is critical. In addition, important aspects concern the physical and economical feasibility of the proposed scheme involving questions related to, for instance, effective local cooling and cost-efficient parallel fabrication of such devices. From a chemist's perspective it is gratifying to note that the first main aspect truly belongs to the realm of synthesis. The unprecedented control over atomic placement controlling molecular shape and properties that can be achieved by the mature art of organic synthesis, in combination with the ever increasing understanding of supramolecular design principles [4], enables the synthetic chemist to play a – perhaps the – key role in the emerging bottom-up approach [5].

Tubular structures (Fig. 1) are among the most versatile functional modules in such nanoconstruction kits [6]. Their inherent geometric features, notably defined inner and outer surfaces as well as termini, give rise to a controlled spatial segregation. This property is associated with a cylindrical dimensionality, which encodes both the directionality necessary for transport processes and the addressability needed for generation of more complex architectures by self-assembly [7] or rational manipulation [8]. Nanotubes can potentially perform a variety of tasks associated with transport of charges and neutral/ionic/chiral species, as well as site-isolation of conducting and/or emitting cores, while at the same time providing the mechanical strength needed for efficient scaffolding. With regard to nanoelectronics, one of the obvious goals is the generation of addressable, insulated nanowires. It should be noted that transport processes could also be coupled to chemical transformations, i.e., catalysis, affording a flow-through nanoreactor for high-end analytic applications.

The synthesis of such functional tubular nanoobjects remains challenging and can be divided into two types of approaches. While the first class is based on the utilization of artificial growth, template, or shape transformation

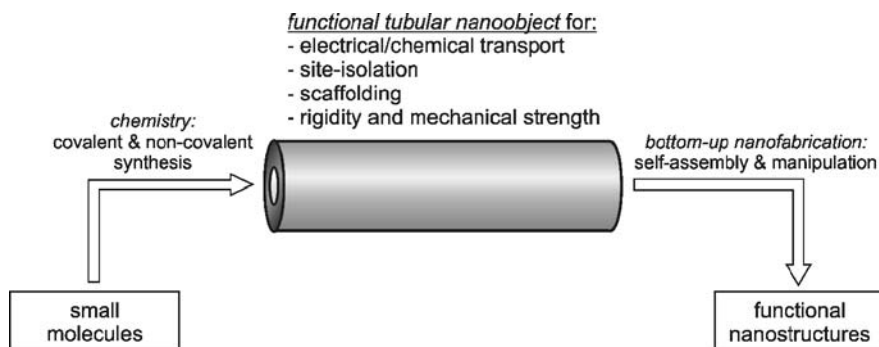


**Fig. 1** Versatility of functional tubular nanoobjects

processes giving rise to the efficient production of carbon and inorganic nanotubes, the second class is founded on a bio-inspired, purely molecular basis. After a brief discussion of general tubular design principles, this review focuses on the latter class of molecule-based synthetic approaches to organic nanotubes [9]. This article primarily covers aspects of covalent and non-covalent synthesis as well as the resulting structural characteristics. For the most part, methods for generating *individual* tubes are presented here, since the nanoobjects have to be addressed separately in order to construct artificial nanostructures. It should be emphasized that due to the fundamental character of this type of research, a detailed discussion of (potential) applications cannot be given. Furthermore, this treatment of the topic can by no means be comprehensive; instead, informed by their personal experiences, the authors have tried to emphasize concepts and present original and significant contributions to this exciting field of research.

## 2 Tubular Design Principles

The information stored in molecular building blocks, such as shape and linkage geometry as well as local solvophilicity/solvophobicity and recognition sites, can be used to generate open-ended hollow tubular objects via a variety of conceptually different approaches (Fig. 2). All approaches use a combination of both covalent and non-covalent syntheses. While defined chemical bonds

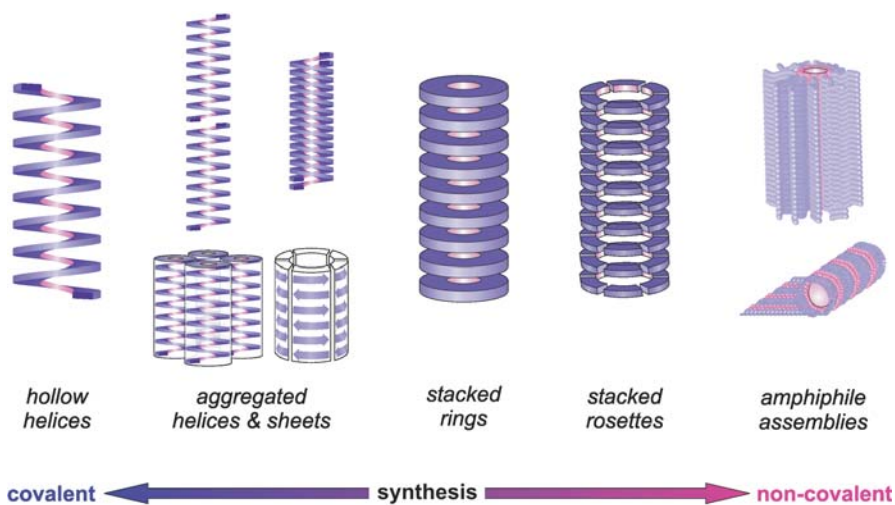


**Fig. 2** General strategies for the design of organic nanotubes based on hollow helical scaffolds and their self-assembly, stacks of macrocycles and rosettes, as well as cylindrical micelles and rolled bilayer sheets

provide both increased stability and control over molecular conformation, supramolecular interactions allow for ease of synthesis and repair of defects. These advantages are accompanied by significant challenges concerning, for instance, efficient and large-scale covalent synthesis on the one hand and predictability of structure formation in self-organizing systems on the other.

The approach with the uppermost covalent character relies on generating helices containing an internal void channel. Hereby, non-covalent interactions are only used to control secondary helical structure formation in the case of folding backbones. Multiple helical entities can be organized in three different modes, namely, they can intertwine to form multi-stranded helices, stack along their axis in continuous fashion to afford tubes, or align parallel to each other to yield bundles. A related motif arises from the aggregation of  $\beta$ -sheets to form barrels. Reduction of the helical to a cyclic motif and introduction of face-to-face non-covalent interactions leads to tubes based on stacked rings. By establishing additional orthogonal non-covalent interactions, the cyclic moiety itself can be formed by self-assembly from sector-shaped units, and the resulting rosettes arrange in a stacked fashion. Finally, the ultimate self-assembly approach is based on either cylindrical micelles or rolled sheets arising from certain amphiphiles and curved bilayers, respectively. Regioselective covalent crosslinking [10] of the tubular architectures proves to be a valuable means to permanently stabilize the frequently rather fragile objects. In principle, the approaches outlined above allow for precise control over dimensions and local chemical functionality of the resulting tubular structures. This is of the utmost importance for incorporating such nanoobjects into more complex nanostructures.

Before discussing these molecular approaches to obtain organic nanotubes in this order, alternative processes for generating carbon [11, 12] and inorganic [13] nanotubes should briefly be mentioned. The many possible preparation strategies are mainly based on one-dimensional growth processes, template-directed syntheses, and shape transformations [13]. Polymer nanotubes have also been prepared using various template-based approaches [14, 15]. In an analogy to the creation of chiral tubes from folded bilayer sheets (*vide infra*), it is interesting to note that the different electronic properties of single-walled carbon nanotubes can be related to the directions in which a graphene sheet is folded. It should be emphasized that currently, carbon (and inorganic) nanotubes represent perhaps the most promising building blocks for the future bottom-up approach [16] because of the tubes' exceptional properties as well as their commercial availability. Current drawbacks consist mainly of separation/purification issues and the solely statistical, i.e., not regioselective, functionalization of the tubes' peripheries [17, 18].

### 3

## Tubes from Hollow Helical Backbones

The helix is among the most abundant structural motifs in Nature due to its inherent chirality and advantageous geometric features (*vide supra*). Oligonucleotide helices in the form of double-stranded DNA are responsible for storing and copying the genetic information, and therefore carry out one of the most essential tasks in the organization of life. Peptide helices perform diverse biological functions including: (1) molecular recognition at the helix surface owing to the well-defined arrangement of amino acid side chains, for instance mediating the Bak peptide – Bcl-x<sub>L</sub>-protein interaction that regulates cell apoptosis related to the development of cancer [19]; (2) selective chemical transport through the helical interior due to transmembrane-channel-forming properties, illustrated by the gramicidin A channel [20]; (3) mechanical strength due to formation of supramolecular superhelical fibers, for instance in the triple helical, bundled collagen cable [21]; and (4) scaffolding due to its inherent rigidity and well-defined binding sites, for instance used for the arrangement of the different bacteriochlorophyll pigments in the light-harvesting complex II in bacteria [22]. The astonishing variety of naturally occurring helical motifs serves as inspiration for the design of artificial helices.

Helical backbones are either inherently stiff due to molecular arrangements such as linkage geometry and steric requirements, or they represent thermodynamically favored helical conformations (foldamers). The first class mostly consists of helical rods having no internal void, reflected in well-known helical polymers [23] such as poly(isocyanide)s or poly(phenylacetylene)s. In the case of foldamers [24], the conformational preference is dictated by non-covalent interactions between neighboring and/or non-neighboring repeat units as well as entropic factors. The reversible helix-coil transition allows population of the global minimum structure and therefore provides a means to repair local defects. The existing fine balance between secondary structural elements is one of the key requirements for the hierarchical structure evolution in Nature. However, from a materials standpoint, this reversibility might also constitute a disadvantage with regard to structural integrity and hence device stability/lifetime under a variety of environmental conditions.

Synthesis of such helical scaffolds is accompanied by their critical structural characterization. X-ray crystallography has proven to be among the most useful tools for elucidating helical structures in the solid state, while in solution a variety of techniques have been employed. In addition to various NMR spectroscopic methods that provide important information on neighboring interactions, CD spectroscopy has been instrumental in monitoring (excess) helicity. In certain cases, UV/vis absorption as well as fluorescence techniques have been used as complementary analytical tools.

In this section, *hollow* helical backbones are reviewed according to their design features responsible for helix formation. For comprehensive treatments

of helical polymers and foldamers, respectively, the reader is referred to the excellent reviews by Nakano and Okamoto [23] as well as Moore and co-workers [24].

### 3.1

#### Inherently Stiff [*n*]Phenylene Helices

The classical helicene structure [25, 26] containing no inner cavity can be extended by introduction of cyclobutadiene fragments into the *meta*-annulated benzene ring system to afford angular, and finally helical, [*n*]phenylenes ( $n \geq 6$ ). The internal diameter of the helix measures 4.0 Å [27]. It should be noted that this backbone is inherently stiff and helical owing to strong covalent interactions introduced by the mode of ring annelation. Vollhardt and coworkers recently realized the synthesis of several helical [*n*]phenylenes derivatives with  $n=7-9$  [28, 29]. The elegant syntheses are based on either twofold or threefold intramolecular cobalt-catalyzed [2+2+2] cyclotrimerization reactions of various phenylacetylene derivatives (Fig. 3).

These moderately air-stable, orange-colored [*n*]phenylenes can be crystallized, for instance [8]phenylene adopts right- and left-handed helical conformations in the solid (Fig. 4). For [7]phenylene **1**, variable temperature NMR experiments indicate a surprisingly low activation energy of 12.6 kcal/mol for helix reversal in solution rendering an enantiomeric separation infeasible.

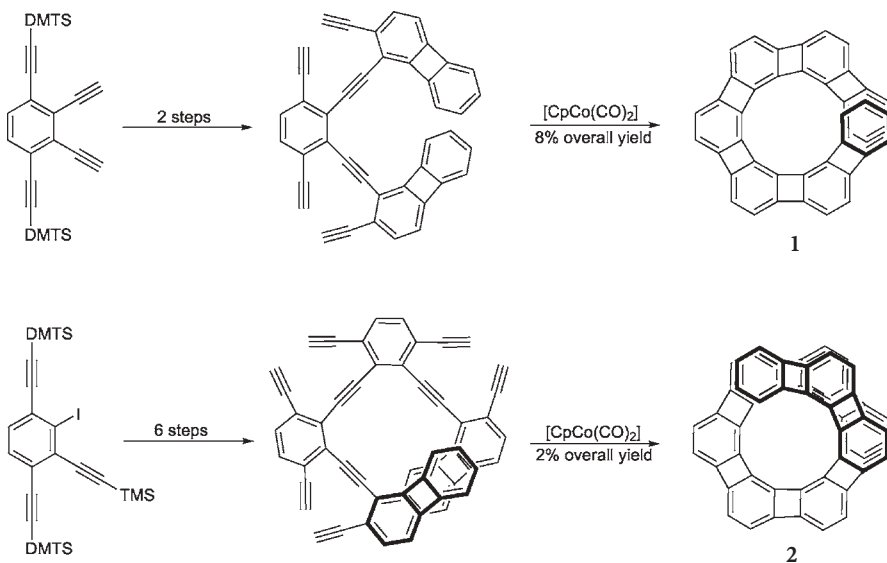


**Fig. 3** Vollhardt's synthesis of [7]phenylene **1** and [9]phenylene **2** by multiple intramolecular [2+2+2]cyclotrimerization reactions. *DMTS* Dimethylhexylsilyl, *TMS* trimethylsilyl

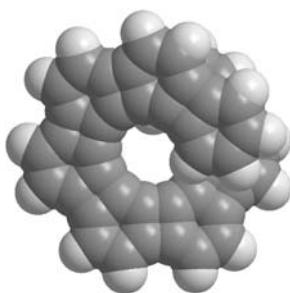


**Fig. 4** Crystal structure of [8]phenylene (CCDC-183203)

## 3.2

### Helical Backbones Based on Intramolecular H-Bonding

#### 3.2.1

##### Alternating D,L- $\alpha$ -Peptides

Secondary structural preferences in peptides are governed by the inherent rigidity of the amide bonds, which significantly reduces the number of accessible conformations, as well as directing and stabilizing intramolecular H-bonding interactions. The antiparallel amide segments are connected by the asymmetric carbon atom carrying the amino acid side chain, and therefore two important dihedral angles  $\Phi$  and  $\Psi$  are defined (Fig. 5). The most abundant secondary structural motifs found in peptide sequences are the  $\beta$ -sheet and the  $\alpha$ -helix.

In an idealized  $\alpha$ -helical conformation ( $\Phi=-57^\circ$ ,  $\Psi=-47^\circ$ ), the side chain residues radiate outward and 3.6 repeat units constitute one turn. This is owing to an intramolecular H-bond between the carbonyl oxygen atom in position  $i$  and the amide proton in position  $i+4$  giving rise to a 13-membered ring, and the  $\alpha$ -helix is hence referred to as a  $3.6_{13}$ -helix. The inner walls of an  $\alpha$ -helix are in van der Waals contact so that the structure contains no inner void. Slightly different dihedral angles ( $\Phi=-60^\circ$ ,  $\Psi=-60^\circ$ ) cause the formation of an alternative  $3_{10}$ -helix having a smaller outer diameter.

In an idealized  $\beta$ -strand composed of all L-amino acids ( $\Phi_L=-120^\circ$ ,  $\Psi_L=+120^\circ$ ), the arrangement of adjacent residues causes the direction of the peptide backbone to alternate in a sinusoidal fashion. Therefore, a peptide composed of alternating D- and L- $\alpha$ -amino acids can adopt a stable  $\beta$ -helical conformation stabilized by  $\beta$ -sheet-type H-bonding [30]. In an idealized  $\beta$ -helix ( $\Phi_L=-133^\circ$ ,  $\Psi_L=+117^\circ$ ;  $\Phi_D=+118^\circ$ ,  $\Psi_D=-130^\circ$ ) the amino acid side chains are pointing outward, leaving a central pore running along the helix axis. The diameter of the inner channel is strongly influenced by the helix periodicity and the number of residues per turn. Computational studies show that single stranded  $\beta$ -helices with 4.8, 6.2, and 8.2 residues per turn should display pore diameters of 2.3, 3.3, and 4.7 Å.

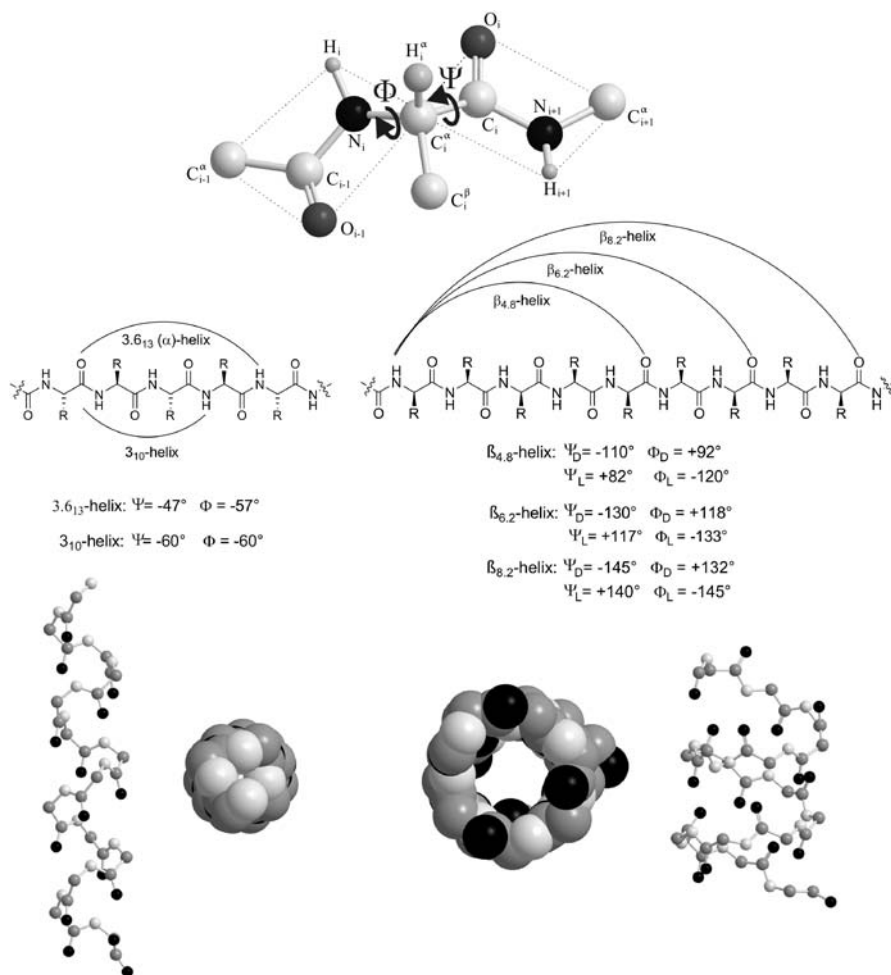


**Fig. 5** Conformational preferences of an  $\alpha$ -peptide backbone giving rise to either an  $\alpha$ - or  $\beta$ -helix depending on the chirality of the amino acid building blocks. Models show top and side views of an idealized  $\alpha$ -helix (*left*) and the  $\beta$ -helix of gramicidin A (*right*) (pdb code: 1MAG; O-atoms are *black*, C-atoms are *gray*, N-atoms are *light*; H-atoms are omitted for clarity)

In addition, a variety of alternative helical conformations exist in these and other peptides composed of non-natural amino acids.

### 3.2.2 Aromatic and Heteroaromatic Amides

In contrast to peptide helices, H-bonding interactions between adjacent repeat units can be used to organize the backbone into a (continuously) kinked con-

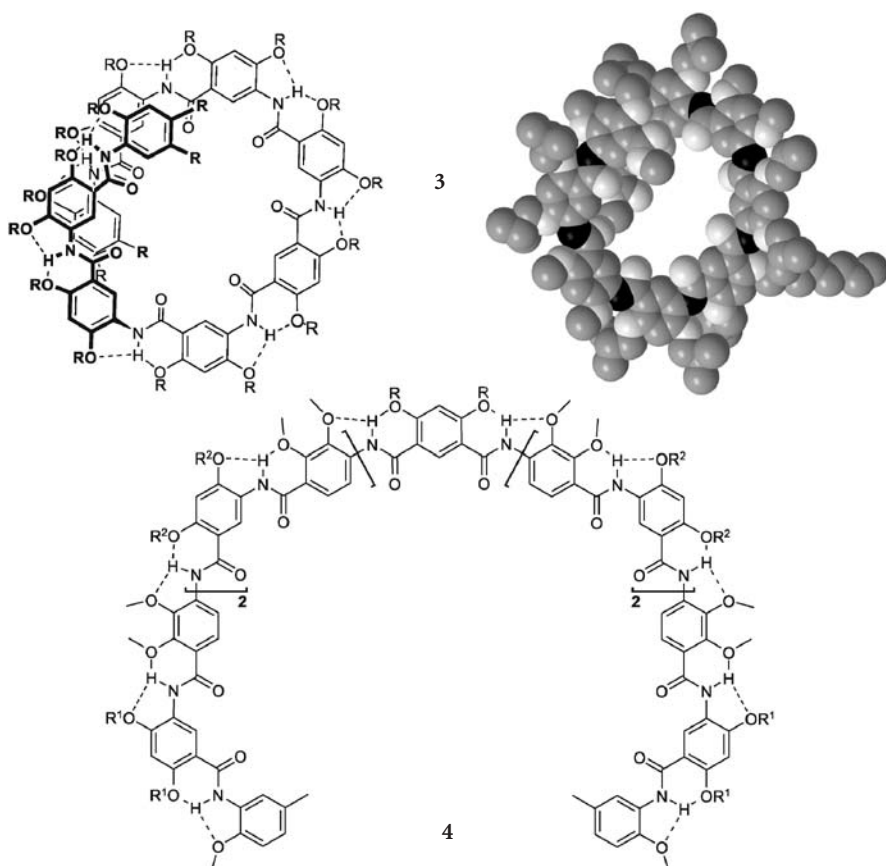


**Fig. 6** Gong's helical diarylamides of varying diameter depending on their mode of connectivity. Crystal structure of *meta*-linked diarylamide 3 (CCDC-188141; O-atoms are light, C-atoms are gray, N-atoms are black; H-atoms are omitted for clarity)

formation that at a certain backbone length affords a helical structure. In the case of aromatic amides [31], further stabilization arises from  $\pi,\pi$ -stacking interactions between overlapping (non-neighboring) repeat units of adjacent turns.

The first reported systems by Hamilton and coworkers are based on a sequence of alternating anthranilamides and 2,6-pyridinedicarboxamides [32–34]. Several oligomers were shown to adopt stable helical conformations in the crystal and in solution. However, these foldamers do not contain a significant internal cavity due to their internal H-bonding motif.

In order to obtain hollow crescent and helical structures (Fig. 6), Gong and coworkers investigated *meta*-linked diarylamides 3 sharing three-center H-bonds at the external rim [35]. One turn consists of six repeat units and the inner hydrophilic cavity has a diameter of 8.2 Å [27], as confirmed by X-ray crystallographic analysis (Fig. 6) [36]. In solution, 2D NMR NOESY experiments

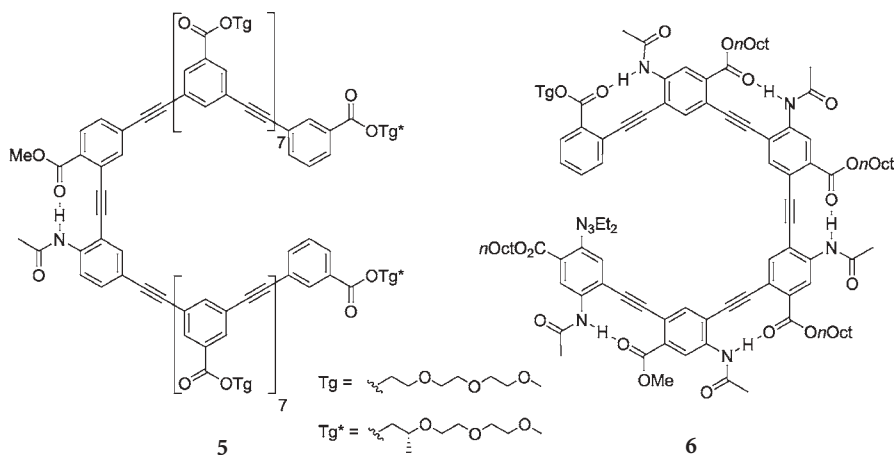


**Fig. 7** Stabilization of helical oligo(*meta*-phenyleneethynylene)s by either single or multiple peripheral H-bonding interactions

show strong interactions between the terminal methyl groups and both aromatic and amide protons of the overlapping turn in the case of the nonamer. The internal diameter can be modulated by insertion of *para*-connected repeat units [36]. The resulting alternating *meta*-/*para*-diarylamide oligomers **4** possess an increased pore diameter of  $\sim 25\text{--}30$  Å. Inserting additional *para*-connectors further increases the inner cavity yielding an astonishing inner diameter of  $\sim 50$  Å in the case of an alternating *meta*-/*para*-/*para*-diarylamide backbone. This strategy to tune the helix diameter by linkage geometry [37] resembles Lehn's approach to various *trans*-2,2'-bipyridine-based helical backbones (*vide infra*).

The helical conformation of *meta*-phenylene ethynylene oligomers can be stabilized using an external H-bonding motif between adjacent repeat units. This has been accomplished by incorporating either single [38] or multiple [39] H-bonding interactions (Fig. 7). When one H-bonding unit was present, the helix stability of backbone **5** carrying polar triglyme side chains was increased by  $\sim 1$  kcal/mol in acetonitrile, as indicated by solvent denaturation experiments. Introduction of these stabilizing interactions between every repeat unit of the same backbone having non-polar side chains (**6**) leads to helical structure formation in chloroform, as indicated by the observed NOE signals of end-to-end contacts. The cavity of the folded structures in both cases resembles the one of the amphiphilic *meta*-phenylene ethynylene foldamer family (*vide infra*) and amounts to  $\sim 7$  Å [27].

Huc, Lehn, and coworkers have carried out detailed studies on alternating 2',6'-diaminopyridine 2,6-pyridinedicarboxamide oligomers **7** (Fig. 8) [40–42]. In this case, the helical structure has an inner pore of  $3.0$  Å [27] and is caused by internal H-bonding interactions between the pyridine moieties and the amide groups connecting them. The heptamer can dimerize to form double-

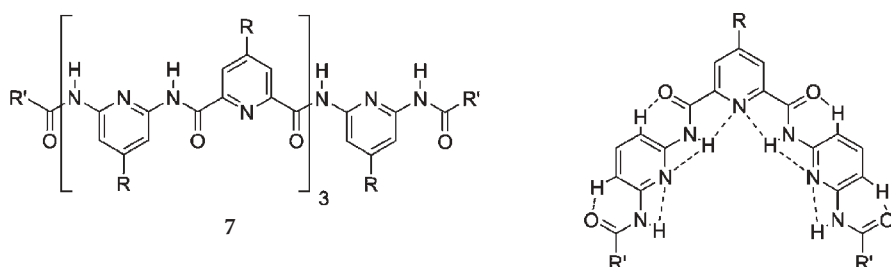


**Fig. 8** Huc's and Lehn's alternating 2',6'-diaminopyridine 2,6-pyridinedicarboxamide oligomers **7** and favored kinked conformation due to H-bonding

stranded helices, which are primarily stabilized by additional intermolecular aromatic stacking interactions, shown by the up-field shift of the aromatic protons in NMR. While a single helix has been crystallized from a rather polar solvent mixture, the corresponding double helix has been obtained by crystallization from a less polar solvent mixture and shows both aromatic stacking as well as H-bonding interactions between the strands (Fig. 9). The system has also been investigated by stochastic dynamic simulations that suggest an enhanced duplex stability with increasing oligomer length. The conformational preference of the backbone is dependent on the protonation of the pyridine units and can therefore be controlled by varying the pH [43, 44]. Recently, an extended quinoline-derived foldamer backbone has been reported by Huc et al. [45]; however owing to the internal H-bonding motif, only a small inner diameter was obtained.

In the case of alternating 2',6'-diaminopyridine isophthalamides, helical structure formation can also be templated by a suitable guest such as cyanuric acid [46]. Molecular recognition is based on triple H-bonding between the

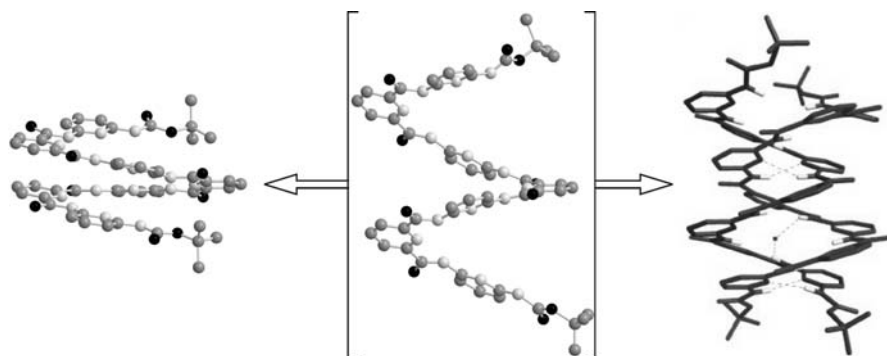


**Fig. 9** Crystal structures of **7** from acetonitrile/DMSO showing a single helix (CCDC-142810) and from heptane/nitrobenzene showing the helix stretching to the double-stranded form and the actual duplex (CCDC-142811; O-atoms are *black*, C-atoms are *gray*, N-atoms are *light*; H-atoms are omitted for clarity). Reproduced in part from [40]

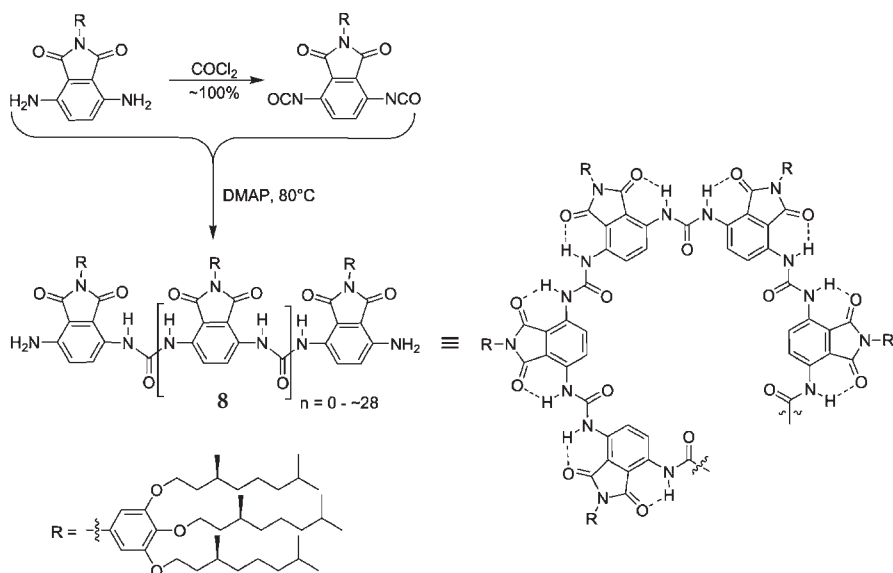


**Fig. 10** Meijer's helically folding ureidophthalimides **8**. *DMAP* Dimethylaminopyridine

guest and the inner rim of the helix as suggested by NMR spectroscopy. Interestingly, the binding process is cooperative, leading to an enhanced affinity for the second guest.

Very recently, ureidophthalimide oligomers and polymers **8** carrying chiral non-polar side groups (Fig. 10) have been described by Meijer et al. [47]. The backbone adopts a helical conformation due to H-bonding interactions between neighboring *anti*-oriented urea and 3,6-disubstituted phthalimide units in combination with  $\pi, \pi$ -stacking between adjacent turns. The helix consists of six to eight repeat units per turn giving rise to an internal cavity of  $\sim 8\text{--}9$  Å in diameter [27]. The chemical shift of the urea protons at 9 ppm indicates intramolecular H-bonding. In CD spectroscopy, oligomers/polymers having more than six repeat units show a Cotton effect in THF. In a competitive H-bonding acceptor solvent such as chloroform no Cotton effect was observed, again illustrating the importance of H-bonding for helical structure formation.

### 3.3

#### Helical Backbones Based on the *trans*-2,2'-Bipyridine Helicity Codon

The preference of 2,2'-bipyridine to adopt a *transoid* conformation has been utilized extensively by Lehn's group to create polyheterocyclic strands with a helical secondary structure. According to computational results, the *cisoid* conformation of 2,2'-bipyridine is destabilized by 5.7 kcal/mol due to repulsion between the *ortho*-protons and lone pairs, while the *transoid* form allows for favorable electrostatic interactions (Fig. 11). Varying connectivity and placement

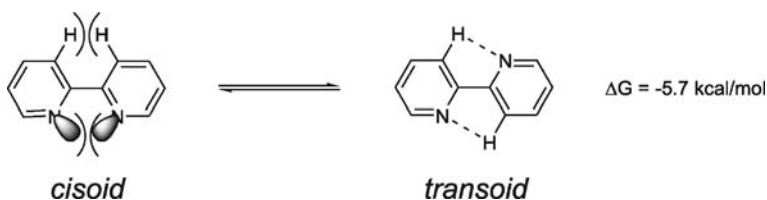


**Fig. 11** Equilibrium between *cisoid* and *transoid* conformations of 2,2'-bipyridine

of the heteroatoms, several foldamer families have been obtained by exploring this design feature, also referred to as 'helicity codon'.

### 3.3.1

#### Alternating Pyridine–Pyrimidine Oligomers

Oligo(pyridine-*alt*-pyrimidine)s constitute the first helical backbone of this type and were described in 1995 [48]. The combination of the above-mentioned preference of 2,2'-bipyridine to adopt a *transoid* conformation, the alternating sequence of pyridine and pyrimidine units with a kinked *meta* connectivity, and intramolecular stacking of overlapping aromatic moieties cause formation of the helical structure. Several oligomers **9** (Fig. 12, left) have been synthesized and investigated. Several X-ray crystal structures were resolved and showed the expected helical conformation [49–52]. In the case of the nonadecamer, the data reveal three complete turns and an interior cavity of 2.5 Å in diameter [27]. Owing to the dynamic helix reversal, chiral crystals contain only one enantiomer.

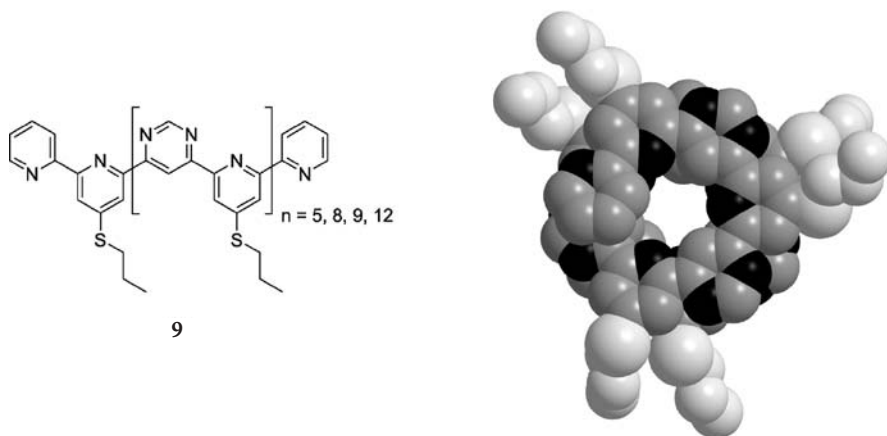


**Fig. 12** Lehn's oligo(pyridine-*alt*-pyrimidine)s **9** and crystal structure of 13mer ( $n=5$ ) (CCDC-100440; N-atoms are black, C-atoms are gray, side chains are light; H-atoms are omitted for clarity)

To investigate the conformational behavior in solution, several techniques have been employed [50, 52]. Extensive NMR studies monitoring up-field chemical shifts of overlapping aromatic protons, measuring NOE signals of interior protons, and utilizing ROESY and COSY methods are all consistent with a helical conformation in solution. UV/vis absorption spectroscopy shows a hypochromic effect indicating stacked chromophores; however, no bathochromic shift was observed. The stacking interaction between chromophores in a helical arrangement is also reflected in the characteristic broad, excimer-like fluorescence emission occurring in oligomers having more than one turn.

The interconversion of the enantiomeric helices has been reported to be fast on the NMR timescale at room temperature in solution. Coalescence temperatures have been used to determine the free energies of activation for helix reversal. Interestingly, they seem to be rather independent of chain length ( $12.3 \leq \Delta G^\ddagger \leq 13.6$  kcal/mol), suggesting a stepwise mechanism for helix inversion [50, 52].

Upon addition of metal ions, the 2,2'-bipyridine-containing helices can undergo a significant structural reorganization, i.e., expansion, forming grid-type architectures. This transition can be reversed by addition of a stronger chelating ligand, which can be either masked or activated by decreasing or increasing the pH. Therefore, a system capable of reversible molecular motion potentially suitable for designing nanosized machines can be realized [53, 54].

The pyridine heterocycle within the helicity codon can be mimicked by a hydrazone unit that, in analogy, stabilizes the *transoid* conformation yet offers the advantage of facilitating synthesis. Incorporation of hydrazone units has been

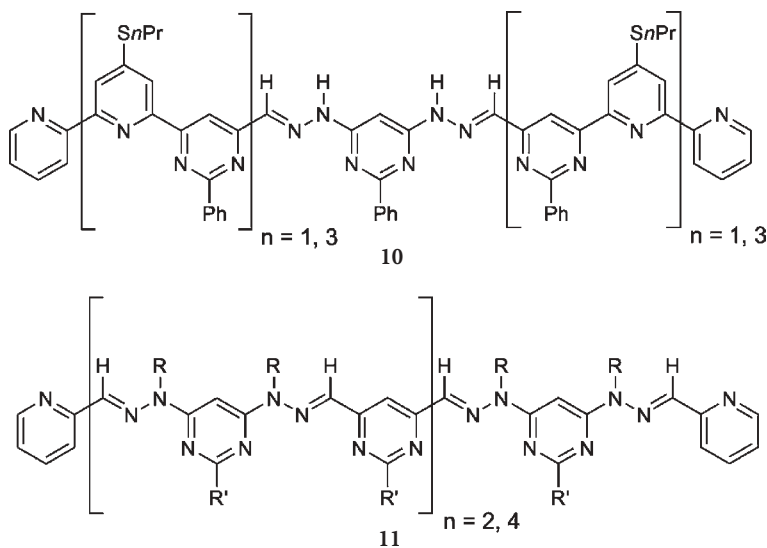


**Fig. 13** Incorporation of hydrazone units to mimic the pyridine heterocycle in the center (10) or throughout the sequence (11)

accomplished either in the center of the backbone [55] or throughout the entire sequence (Fig. 13) [56]. Again, NMR, UV/vis absorption as well as X-ray crystallographic studies demonstrate the helical structure in solution and in the solid state. In the case of oligo(hydrazone-*alt*-pyrimidine)s **11**, phenyl substituents ( $R'$  in Fig. 13) provide additional aromatic stacking interactions and therefore stabilize the helical structure.

### 3.3.2

#### Alternating Pyridine-Pyridazine Oligomers

In order to increase the diameter of the helix, *para*-connected building blocks were introduced and the position of the heteroatoms carefully chosen. The resulting oligo(pyridine-*alt*-pyridazine)s **12** (Fig. 14, top) adopt a helical conformation with 12 heterocyclic units per turn, having a central cavity measuring  $\sim 8\text{--}9\text{ \AA}$  in diameter [27, 57]. In solution, up-field-shifted NMR signals indicate

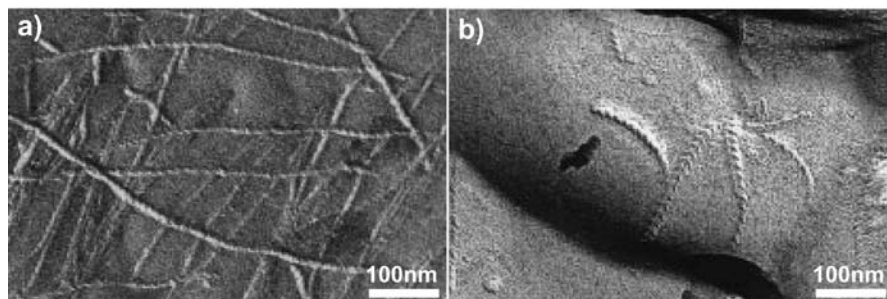
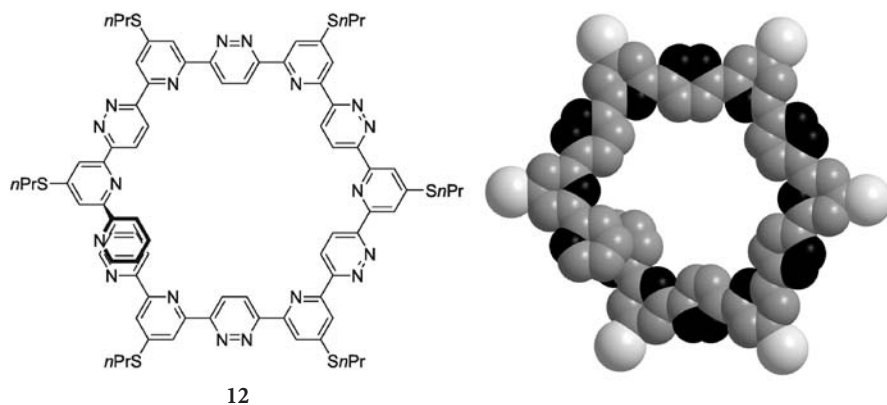


**Fig. 14** Extending the helix diameter using the *para*-connected pyridazine heterocycle to afford oligo(pyridine-*alt*-pyridazine)s **12**. Model (N-atoms are black, C-atoms are gray, S-atoms are light, H-atoms and side chains are omitted for clarity) and freeze-fracture electron micrographs of **12** in  $\text{CH}_2\text{Cl}_2$  (a) and pyridine (b) showing fiber network formation with helical textures. Reproduced in part with permission from [57]

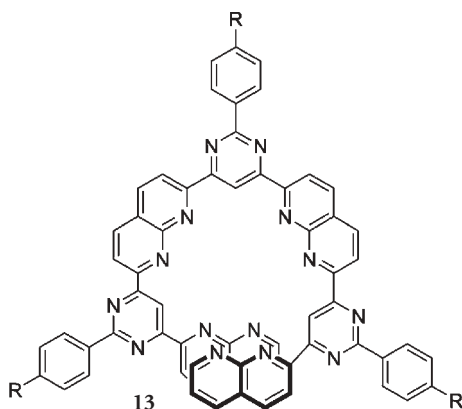


**Fig. 15** Extended oligo(1,8-naphthyridine-*alt*-pyrimidine)s 13 carrying internal chelating ligands

formation of the helical conformation. Interestingly, the aromatic signals are further shifted with increasing concentration pointing to aggregation of the helices. Vapor-pressure osmometry confirms formation of higher aggregates, namely duplexes, in a variety of solvents. Freeze-fracture electron microscopy shows an extensive network of linear and intertwined chiral fibers of high aspect ratio, i.e., micrometer length and  $\sim 80$  Å diameter (Fig. 14, bottom). The fibers are composed of coiled-coil bundles of two or three individual supramolecular helices. The self-aggregation to supramolecular stacks and super-helices is based on intra- and intermolecular  $\pi$ - $\pi$ -stacking interactions between overlapping and neighboring aromatic helix turns.

### 3.3.3

#### Alternating Naphthyridine–Pyrimidine Oligomers

An alternative way to extend the helical structure is to replace the pyridine with naphthyridine units. The corresponding oligo(1,8-naphthyridine-*alt*-pyrimidine)s 13 (Fig. 15) have been synthesized and shown to adopt a helical conformation both in solution and the solid state [58]. The diameter ( $\sim 4$ – $5$  Å [27]) and polarity of the inner cavity allow for interaction with cationic species. Indeed using NMR and ESI MS, it could be shown that cations rapidly induce aggregation of the helical folds in a stacked fashion, forming long interdigitated fibers as evident from TEM.

### 3.4

#### Helical Backbones Based on Solvophobic Forces

In the cases discussed so far, non-covalent interactions inherent in the backbone have been driving helical structure formation. Inspired by the hydro-

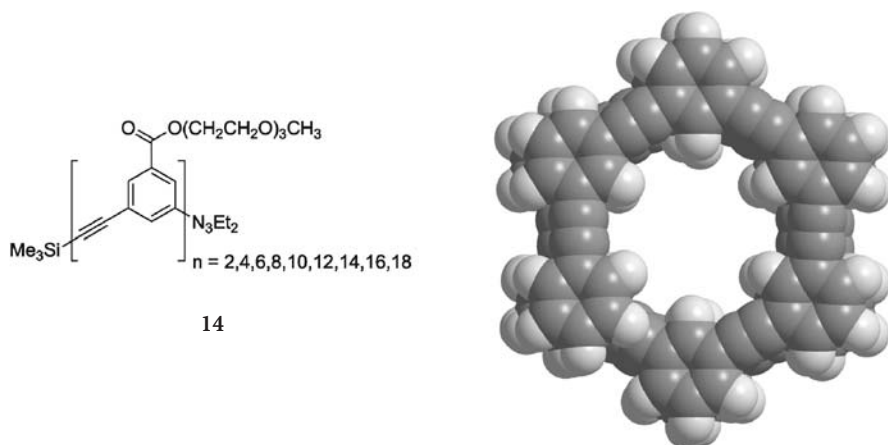


**Fig. 16** Moore's amphiphilic oligo(*meta*-phenyleneethynylene)s **14** and model of the octadecamer (side chains are omitted for clarity)

phobic effect used in Nature to stabilize folded biomacromolecules, amphiphilicity can also be implemented in the backbone to stabilize its helical conformation in solution. Thereby, external solvent leads to segregation of the amphiphilic structure, exposing solvophilic and hiding solvophobic regions of the molecule. In recent years, this design principle has been impressively demonstrated for the case of the amphiphilic oligo(*meta*-phenyleneethynylene) foldamer family **14** (Fig. 16) pioneered by Moore and his group [59].

The helical secondary structure in polar organic solvents such as acetonitrile is caused by the *meta* connectivity of the backbone and  $\pi,\pi$ -stacking interactions between aromatic moieties in adjacent turns, as well as segregation of the polar triglyme side chains and the non-polar phenylacetylene scaffold. In solution, an ESR study investigating line broadening as a function of the number of connecting repeat units between two spin labels suggests that each turn is comprised of six repeat units [60], as expected on the basis of the hexagonal symmetry of related macrocycles (see 5.1.4 and 5.4.1). This conformation gives rise to a tubular cavity measuring  $\sim 7$  Å in diameter [27] (Fig. 16, right). For the structural organization in the solid state see section 4.2.

Given the *meta* connectivity of the backbone, several parameters have been varied and their influence on helix stability investigated. The strength of the  $\pi,\pi$ -stacking interactions can be adjusted by changing the electron density in the aromatic ring system [61, 62]. Only in the case of the electron-deficient ester substituents favoring aromatic stacking helical structure formation could be observed [63]. Additional non-covalent interactions such as H-bonding (see 3.1.2) or interior metal ion binding (*vide infra*) can be implemented in the backbone. Also, the amphiphilicity of the system can be reversed, as illustrated by incorporation of non-polar alkyl side chains that lead to folding in hydro-

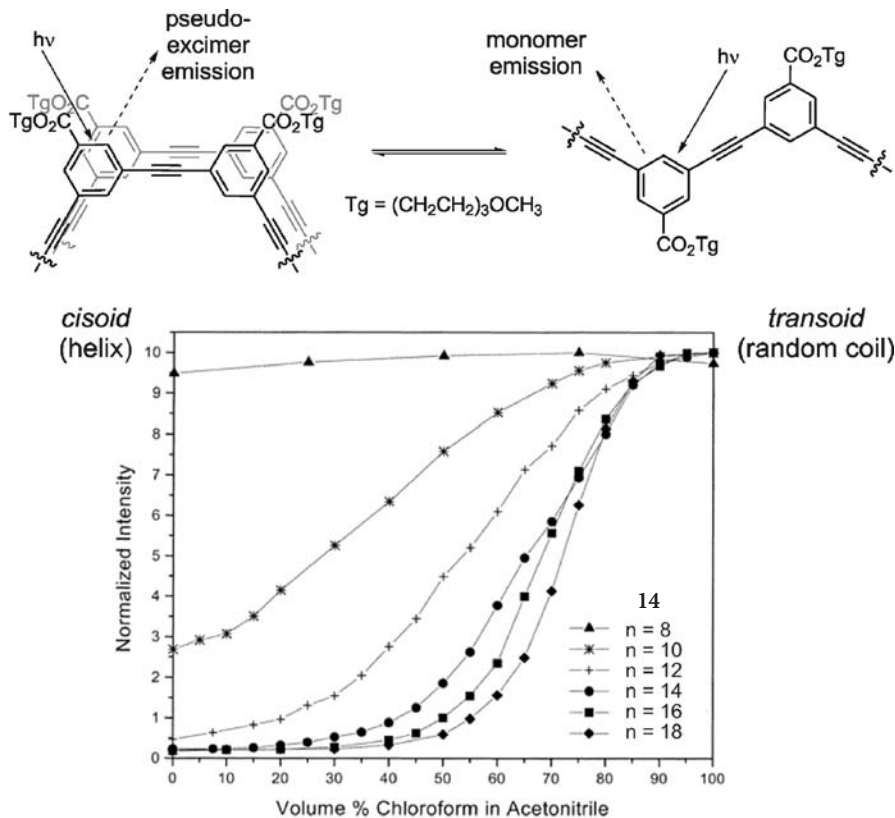


**Fig. 17** *Cisoid* and *transoid* conformations reflecting the helix-coil transition (top). Solvent denaturation experiments demonstrate a chain length dependent, cooperative folding transition in oligomers 14 (bottom). Reproduced in part with permission from reference [66]

carbon solvents [64]. Solvents in general play a critical role and their ability to fold as well as unfold backbone 14 has been studied in detail [65].

Convenient optical monitoring of the conformational transition by means of UV/vis absorption as well as fluorescence spectroscopies has been established for this backbone type (Fig. 17, top) [59, 66]. While *cisoid* and *transoid* conformations display different absorption spectra, isolated and stacked cross-conjugated monomer units show direct or excimer-like emission. The helix-coil transition is temperature-dependent, but is more sensitive to changes in solvent composition. Solvent denaturation experiments show a clear chain-length-dependence of the folding process (Fig. 17, bottom). Starting at the dodecamer, the helix-coil transition both sharpens and shifts to larger amounts of denaturant for higher oligomers. Quantitative analysis shows a linear relationship between chain length and helix stabilization energy, as expected by the helix-coil theory [67]. An incremental stabilization energy  $\Delta G \sim 0.7$  kcal/mol per repeat

unit has been calculated from the data [66]. The observed high degree of cooperativity was quantified and is comparable to that of  $\alpha$ -helix formation in protein folding.

The bias of the twist sense of the helical conformation has been achieved by introducing chiral units, either in the main or side chains (Fig. 18). One of the two resulting diastereomeric helices is energetically favored and causes excess helicity, conveniently monitored by CD spectroscopy. While enantiopure binaphthol segments [68] as well as tartrate-based linkers [69] have been incorporated in the main chain, chiral polar [70] and non-polar side chains [64] have

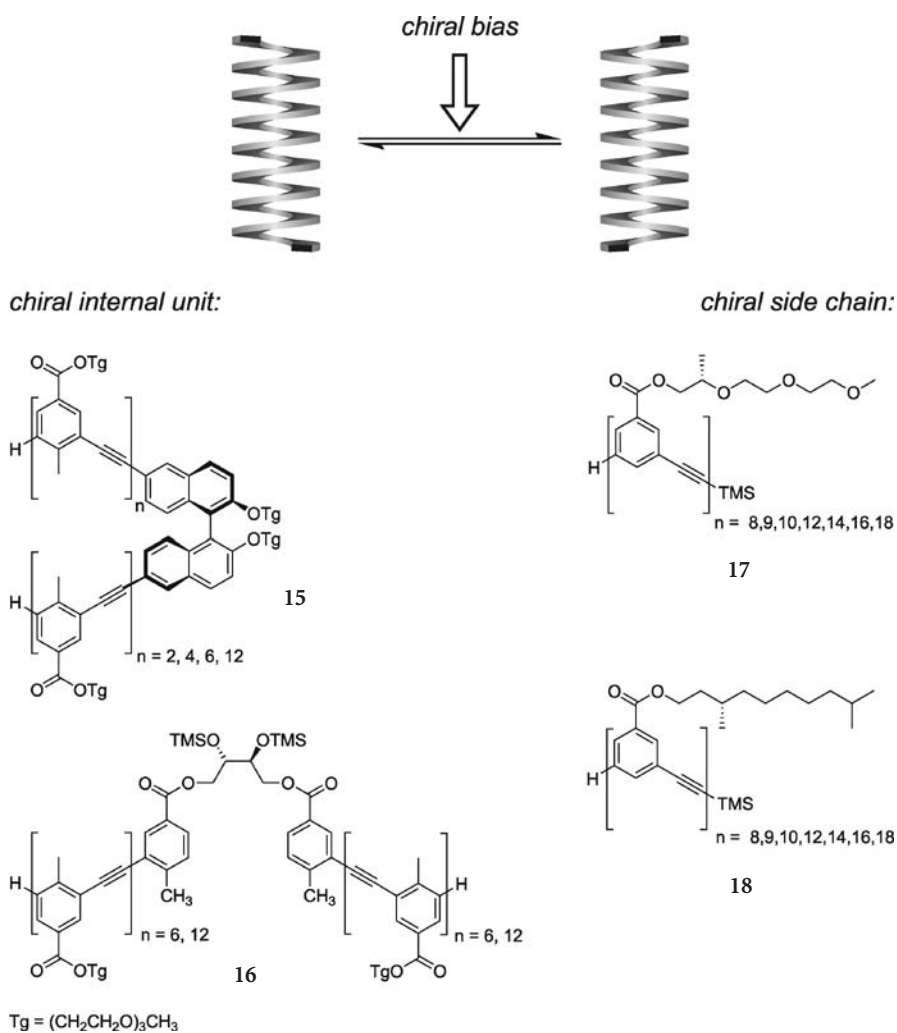


**Fig. 18** Biasing the helical twist sense by covalent incorporation of chirality in the backbone or the side chains. *TMS* Trimethylsilyl

been attached to the backbone as well. Remarkably, a single extra methyl group in the side chain of **17** is able to transfer its chirality to the backbone in a highly cooperative fashion. In “sergeants and soldiers” experiments it was found that the intensity of the CD signal is not linearly dependent on the amount of chiral side chains [71]. Although only a small amount of chiral side chains is needed to induce significant Cotton effects, the values displayed by the corresponding homochiral oligomers could not be achieved.

Host-guest interactions involving guests of complementary size and shape that fit into the inner cavity of the helically folded host have been extensively explored (Fig. 19). For example, the foldamer receptor has been decorated with nitrile functionalities that bind two silver ions at the interior to provide an additional driving force for helical structure formation [72]. Since the coordinating group in **19** was introduced at every other repeat unit, three nitriles per turn can form a favored trigonal planar complex. In another example, induction of chirality has been achieved in polar solvents by binding either  $+\alpha$ -pinene or  $-\alpha$ -pinene in a 1:1 ratio to the internal hydrophobic surface of dodecamer **14** [73]. The resulting enantiomeric complexes have characteristic and opposite CD spectra. Also, the binding of rod-like guest molecules such as *cis*-(2*S*,5*S*)-2,5-dimethyl-*N,N'*-diphenylpiperazine **21** within the tubular cavity was found to be chain length-dependent, indicating that maximizing the area of contact determines affinity [74]. Interestingly, both affinity and chain length specificity for binding the dumbbell-shaped rod **22** were higher than for **21**, illustrating the dynamic nature of the foldamer receptor [75].

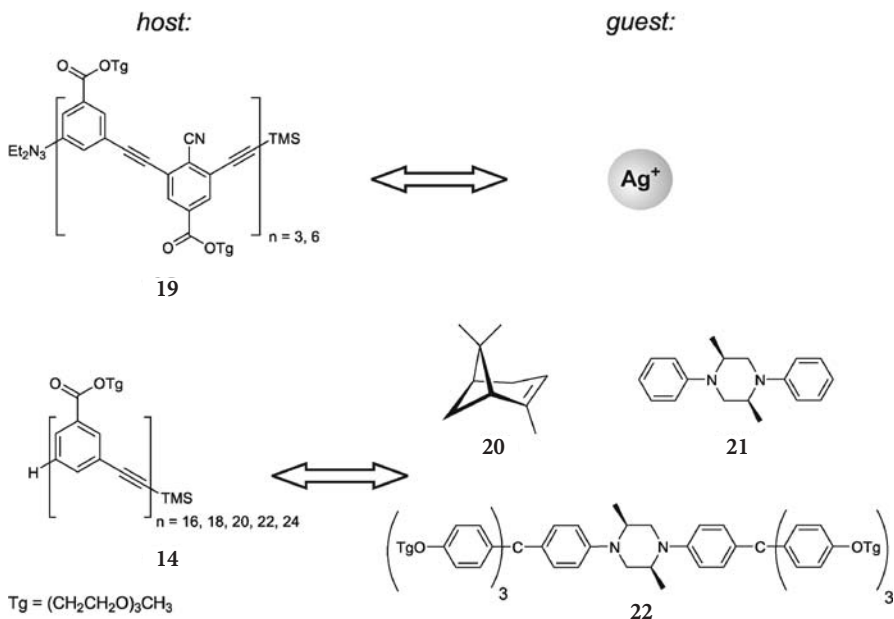


**Fig. 19** Molecular recognition within the interior of dynamic foldamer receptors

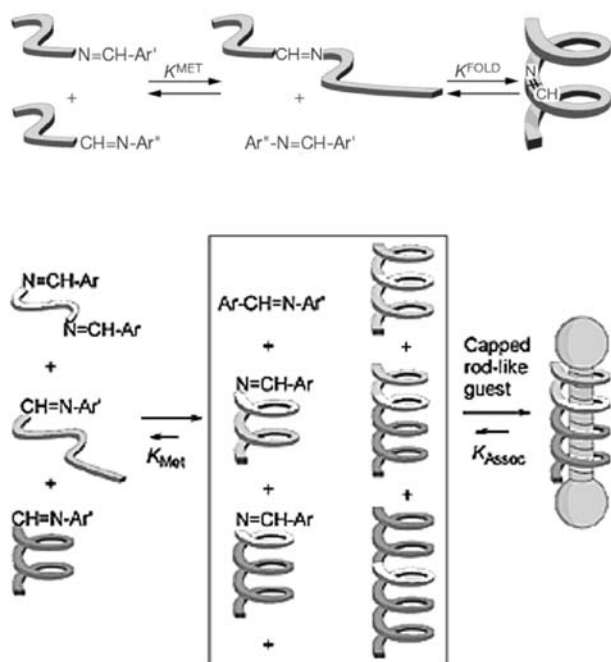


**Fig. 20** Dynamic covalent chemistry by imine metathesis for the synthesis of oligomers via a purely folding-driven ligation reaction (*top*) and a templated, size-selective synthesis (*bottom*). Reproduced with permission from references [77] and [79]

Combining this length-specific binding with dynamic covalent synthesis [76] by taking advantage of reversible imine metathesis, template-controlled, size-selective oligomer synthesis of foldamer receptors has been demonstrated (Fig. 20) [77]. Utilizing further elongated templates, this supramolecular approach should in principle allow for the synthesis of well-defined oligomers of tremendous length. Under equilibrium conditions and in the absence of a template, monomer addition can be driven solely by the free energy gain owing to helix formation [78], as was demonstrated for the case of folding-driven synthesis of oligomers [79, 80] and polymers by imine metathesis [81, 82].

### 3.5

#### Covalent Stabilization by Intramolecular Helical Crosslinking

In order to utilize hollow helical structures in devices that have to operate under changing and sometimes demanding environmental conditions, it might be advantageous to covalently lock the reversibly folding structure by intramolecular crosslinking. Regioselectively crosslinked nanostructures [10] of various topologies are of particular interest in several fields, for instance for the generation of hollow capsules for controlled release applications [83]. However, the

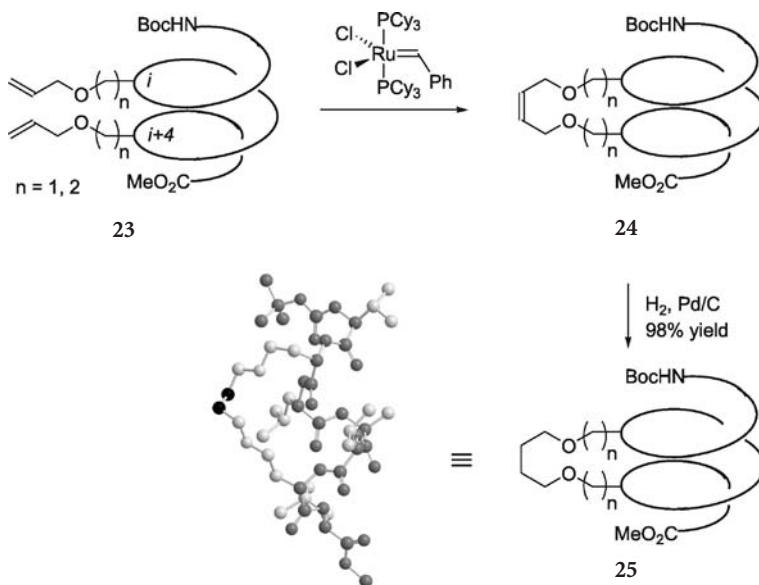


**Fig. 21** Grubbs' introduction of a single covalent crosslink by RCM to stabilize an  $\alpha$ -helical peptide conformation. Crystal structure of **25** (CCDC-101810; ethylene linkages are *black*, helical backbone are *gray*, side chains are *light*, H-atoms are omitted for clarity)

covalent capture of hollow helical conformations has not been explored until very recently.

In one case, Blackwell and Grubbs utilized RCM to introduce a single covalent linkage between two amino acid residues in a short peptide, and thereby stabilize its  $\alpha$ -helical conformation (Fig. 21) [84, 85]. With regard to the context of this review, it is important to note that the  $\alpha$ -helix does not contain an inner void (see 3.2.1). In the heptapeptide sequence Boc-Val-X-Leu-Aib-Val-X-Leu-OMe **23**, the allylated residues X representing serine or homoserine in positions *i* and *i*+4 are located on the same side of the helix, enabling efficient generation of the covalent crosslink. The obtained mixture of olefinic isomers **24** (~5:1 *E/Z*) was subsequently converted to the respective saturated analogue **25**. CD spectra of the linear (**23**) and the cyclic (**25**) peptides in trifluoroethanol do not show noticeable differences, indicating a preorganized helical peptide backbone and negligible structural reorganization during crosslinking. In the case of the shorter, and hence less flexible tether, the X-ray structure revealed a slight conformational change from the initial  $\alpha$ -helix to a  $3_{10}$ -helix. It should be mentioned that Woolley and coworkers have utilized a single azobenzene-containing linker to turn an  $\alpha$ -helical peptide conformation either on or off [86, 87].

In order to obtain stable organic nanotubes, Hecht and Khan recently reported the intramolecular crosslinking of helically folding, hollow, amphiphilic poly(*meta*-phenylene ethynylene)s (Fig. 22) [88]. The lengthy and defect-free

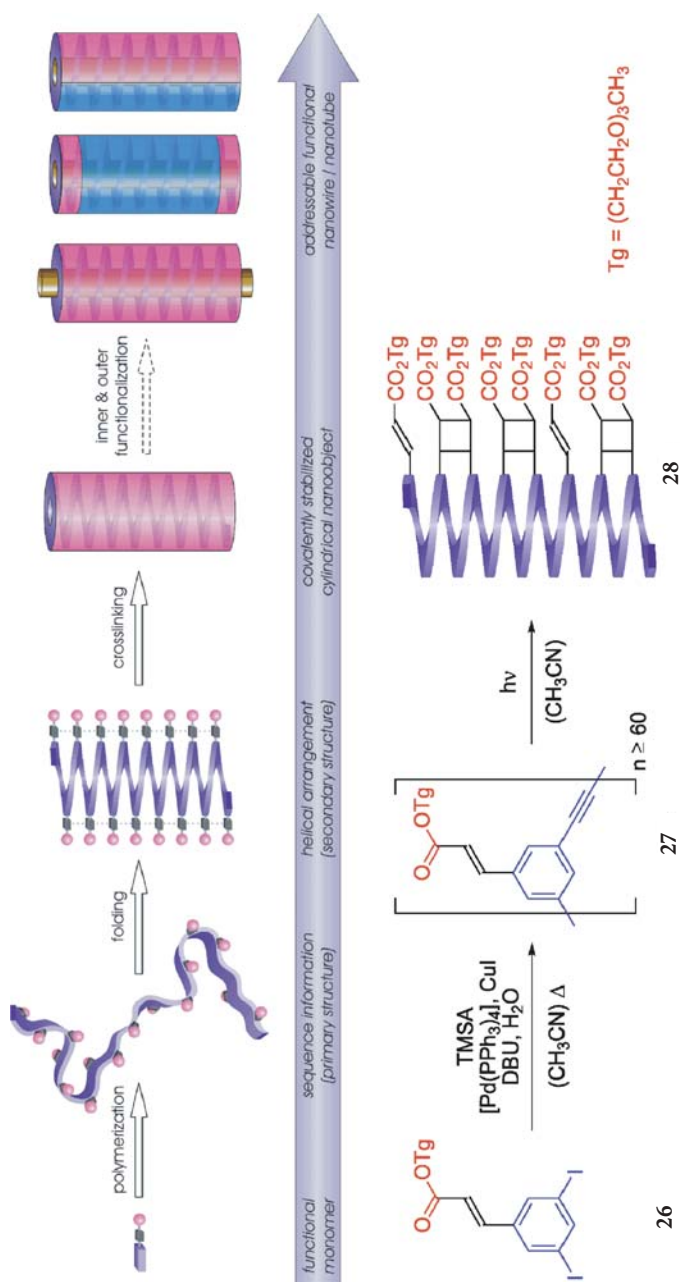


**Fig. 22** Intramolecular crosslinking of helically folded polymers as a route to stable functional organic nanotubes illustrated for poly(*meta*-phenyleneethynylene)s containing photocrosslinking cinnamate groups. *TMSA* Trimethylsilylacetylene, *DBU* 1,8-diazabicyclo [5.4.0] undec-7-ene

polymer **27** was prepared from diiodomonomer **26** via a newly developed  $A_2+BB'$  polycondensation protocol [89]. Taking advantage of the short distances between repeat units in adjacent turns, crosslinking groups were introduced as cinnamates to allow for efficient [2+2] photodimerization. Using the diagnostic tools for the helix-coil transition, well established for the parent oligomer series (see 3.4), stabilization of the helical conformation by means of covalent capture could be demonstrated. Solvent denaturation experiments using UV/vis absorption as well as fluorescence spectroscopies show a typical reversible cooperative folding process for the polymer **27**. Subsequent irradiation of the folded structure of **27** under high dilution conditions leads to incorporation of approximately 20–30% of cyclobutane moieties and the resulting crosslinked helical polymer **28** cannot be unfolded. NMR data indicate the formation of  $\beta$ -truxinates, i.e., *syn* head-head photodimers, and therefore suggest some degree of topochemical control, yet certain structural changes during the crosslinking process cannot be avoided and are evident from the UV/vis titration data and fluorescence spectra. By developing narrow disperse polymerization and introducing proper postfunctionalization, this approach in principle allows for the generation of cylindrical nanoobjects with defined dimensions as well as controlled inner and outer functionality, such as segregated tubes and insulated wires.

## 4

### Tubes from Self-Assembled Helices and Sheets

The state of the art in hollow helical design documented in the last section provides a respectable degree of control over relatively small, unimolecular tubes. However, in order to obtain larger structures, additional non-covalent inter-strand interactions have to be implemented, for instance by intertwining, stacking, or aligning individual helices. In Nature, helical multiplexes are quite common; however, only a few artificial analogues exist. In this section, some examples of helical aggregation modes again focusing on hollow tubular structures are briefly discussed. An excellent review on (supramolecular) helical programming has been given by Nolte and coworkers [90].

#### 4.1

##### Multi-stranded Helices

The most compact mode of helical aggregation arises from intertwining two or more helices to afford double or multi-stranded helices. Double-stranded DNA constitutes the prototype of a helical duplex. Both strands are held together by interstrand H-bonding interactions between the complementary base pairs that largely determine the stability of the duplex. Although it may seem obvious, the location of the bases at the helix interior precludes the use of DNA as a tube with an exploitable inner cavity. Another naturally occurring example involves

double-stranded gramicidin D complexes that, although displaying a rather high pitch, form channels of considerable diameter (4.8 Å) [91]. Artificial systems such as Lehn's helicates, i.e., artificial duplexes based on coordination of two ligand strands around a central string of metal ions, are not hollow and the reader is referred to the numerous reviews on this topic [92–94]. One example of double helix formation has already been presented in the case of **7** (see 3.2.2), but again the inner void is rather small. To our knowledge, intertwined multiplexes generally do not contain a considerable unoccupied inner cavity and hence will not be discussed in this section.

## 4.2

### Stacking Helices

In order to increase the aspect ratio of covalently synthesized helices, where the length that can realistically be achieved is limited by the efficiency of chemical bond formation, helices can be stacked on one another in a continuous fashion to generate hollow tubes. The gramicidin A dimer represents a naturally occurring example of such a self-assembled stacked helix motif that spans the cell membrane and acts as an ion channel [20]. Both helices are held together by end-to-end H-bonding contacts that direct aggregation. Stacking of helices has been noted in some artificial systems including Lehn's alternating pyridine-pyrimidine (see 3.3.1) and pyridine-pyridazine oligomers (see 3.3.2) as well as Moore's *meta*-phenylene ethynylene foldamers (see 3.4). In the latter case, it was shown that the mode of aggregation in the solid state is dominated by packing effects [95–97]. While the parent oligomer series **14** aggregates in a lamellar structure to minimize the void volume that would be created by stacking helices, the *endo*-methylsubstituted series **29** forms a hexagonal columnar structure since the helix interior is occupied (Fig. 23).

Helical aggregation of oligomers **17** also occurs in aqueous acetonitrile solution and plays an important role in the context of hierarchical chirality transfer [71]. The side chains induce excess helicity and (chain length dependent) aggregation into chiral columns results in the reversal of overall chirality.

## 4.3

### Bundles

Tubular structures with, in general, relatively small inner channels are realized by ordered  $\alpha$ -helical bundles. Peptitergents, vertically segregated, amphiphilic  $\alpha$ -helical peptides, can arrange in a columnar fashion to generate helix bundles having either hydrophilic or hydrophobic inner cavities. In Nature, these bundles are frequently constructed in an intramolecular fashion from individual helical segments of a single large protein that are connected by loops [98]. Perhaps the most investigated example is the potassium channel (Fig. 24, top left) with a void diameter of  $\sim 6$  Å at the selectivity filter region, i.e., the narrowest segment [99]. Rational design of the amino acid sequence enables fine-tuning

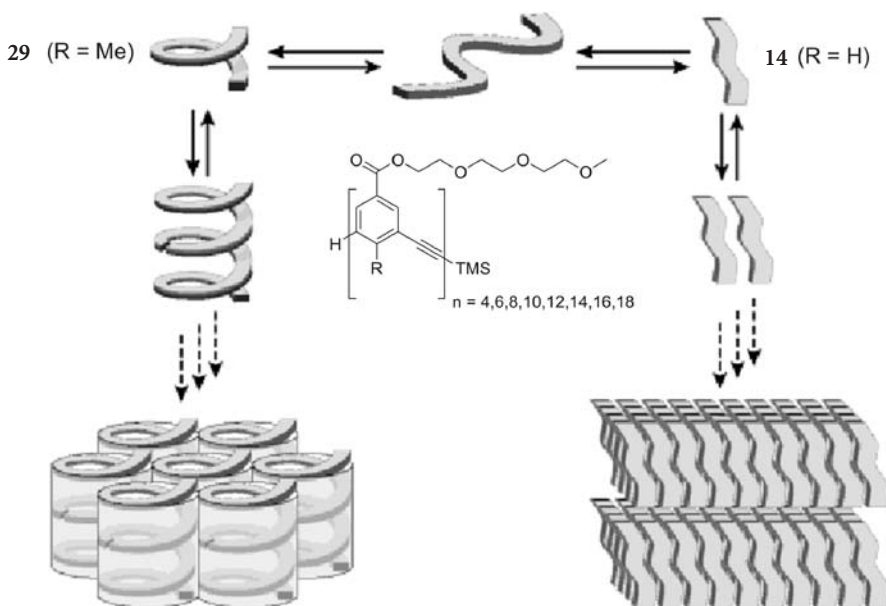


**Fig. 23** Balance between lamellar and columnar solid-state aggregation in oligo(*meta*-phenyleneethynylene) series 14 and 29. Reproduced in part with permission from reference[97]

of the axial segregation ratio and local electrostatics and therefore allows for the design of tubular objects with varying numbers of  $\alpha$ -helices and defined inner and outer surfaces. For example, four-helix bundles with lengths of 3.5 nm display inner void diameters of only 1.5 Å [100]. In contrast, arrays of a larger number of helices can exhibit inner diameters beyond 1 nm [101].

#### 4.4 Barrels

In addition to forming  $\alpha$ -helix bundles, peptide-based systems assemble into related tubular motifs such as  $\beta$ -barrels [102].  $\beta$ -barrels are constructed from staves consisting of  $\beta$ -sheets. In biological systems, the assembled staves are arranged in a slightly twisted manner and usually, as the name indicates, contain a barrelhead. Most barrels are formed by a single large protein having several interconnected  $\beta$ -strand segments [103, 104]. For example,  $\alpha$ -hemolysin (Fig. 24, top right) consists of a heptameric barrel with a large inner diameter of 2.5 nm [105]. Artificial rigid-rod  $\beta$ -barrels **30** based on stiff oligo(*para*-phenylene)s carrying short peptide side chains have been described by Matile and coworkers (Fig. 24, bottom) [106]. Covalent preorganization of the staff's shape by using a rigid rod-like backbone combined with the formation of an interdigitating antiparallel H-bonding array between the peptide fragments

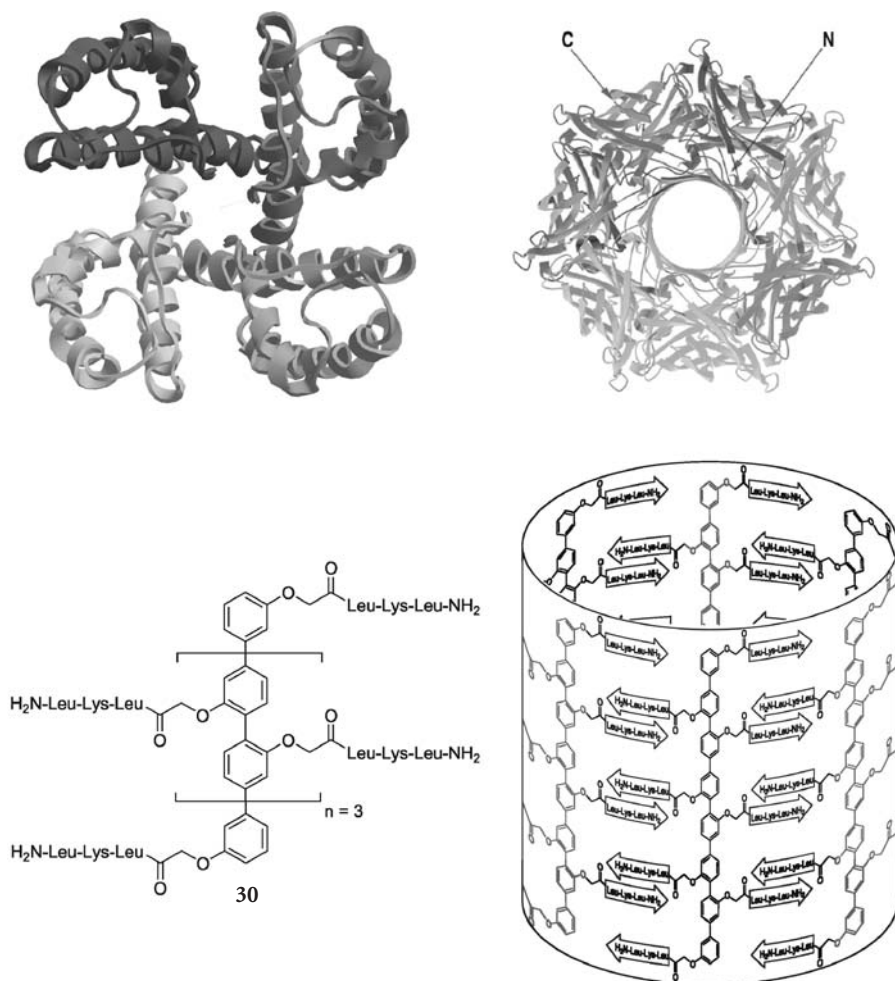


**Fig. 24** Crystal structures of naturally occurring bundles and barrels: the potassium channel (pdb code: 1BL8, *top left*) and  $\alpha$ -hemolysin (*top right*). Matile's rigid-rod  $\beta$ -barrels **30** composed of oligo(*para*-phenylene) rods with  $\beta$ -strand forming short peptide side chains (bottom). Reproduced in part with permission from reference [105]

proves to be an efficient strategy for creating hollow nanostructures with defined interior functionality. Most likely, hexameric barrels measuring 3.4 nm in length and  $\sim 1$  nm in internal diameter are formed [107]. The barrel dimensions can be tuned by the number of staves as well as by the length of the peptide side chains; for instance, 2–6 staves encode inner diameters of 2–25 Å [106]. The transmembrane activity of rigid-rod  $\beta$ -barrels has recently been exploited for designing a high-throughput fluorometric detection system of enzyme activity [108].

## 5 Tubes from Stacked Macrocycles

One way to create hollow tubular structures is the self-assembly or stacking of rings. In this design concept, covalent bonds encode the inner and outer diameters of the tube while non-covalent interactions control the length of the object. Intermolecular interactions responsible for continuing association in a stacked fashion include H-bonding, aromatic  $\pi,\pi$ -stacking, and solvophobic forces. It is interesting to note that although this ring-stacking motif has been utilized extensively to design artificial tubular systems, related cases are not common in Nature. In this section, the tubular structures are discussed depending on environmental conditions, i.e., phases, and backbone types. Furthermore, covalent stabilization of the assembled objects will be described. Due to the topological resemblance, tubes based on cored, dendronized polymers have been included in this section. Related metal complexes of some cyclic ligands and their discotic self-assembly have been omitted since the metal occupies the inner void of the system. For further information on (hetero)aromatic macrocycles, the reader is referred to recent comprehensive reviews by the groups of Höger [109], Moore [110], and Schlüter [111].

### 5.1 Tubular Structures in the Solid State

#### 5.1.1 Cyclic Peptides

As early as 1974, DeSantis et al. recognized that peptides having an even number of alternating D- and L-amino acids displaying  $\beta$ -type dihedral angles could in theory form closed rings, which can generate hollow cylinders by stacking through intermolecular H-bonding interactions [30]. Almost two decades later Ghadiri and coworkers demonstrated this concept as they designed, synthesized, and studied alternating cyclic peptides **31** (Fig. 25) [112, 113].

Upon acidification of alkaline solutions of *cyclo*-[-(L-Gln-D-Ala-L-Glu-D-Ala)<sub>2</sub>-], rod-shaped crystals having a high aspect ratio with average dimensions of 10–30  $\mu\text{m}$   $\times$  100–500 nm were formed. Each crystal consists of an organized bundle of hundreds of tightly packed nanotubes. A variety of experimental methods including TEM, cryo-TEM, and electron diffraction as well as molecular modeling show that the tubular stack has an inner diameter of 7 Å and a 4.7 Å axial periodicity. This intersubunit distance corresponds to an ideal antiparallel  $\beta$ -sheet conformation, which is further supported by the observed N–H-stretching frequency at 3,277  $\text{cm}^{-1}$ , indicative of strong H-bonding interactions. In this  $\beta$ -sheet-type arrangement, all amino acid side chains are located at the periphery, affording a polar inner cavity. It should be noted that these peptide crystals display good mechanical and chemical stability.

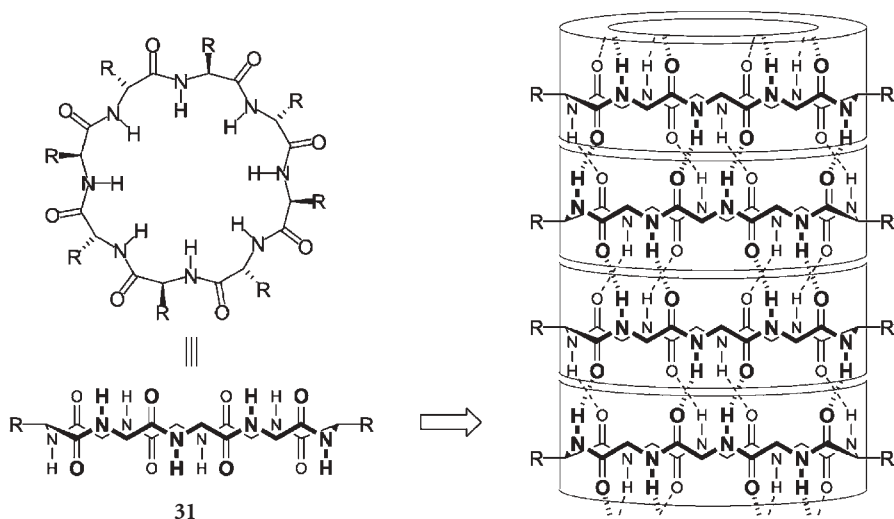


**Fig. 25** Ghadiri's self-assembling nanotubes based on cyclic  $\alpha$ -peptides 31 consisting of alternating D- and L-amino acids

The versatility of Ghadiri's approach arises from the fact that the internal diameter (at least within a certain range) and the properties of the outer surface can easily be modified by adjusting the ring size and introducing various amino acid residues. For example, cyclopeptides containing either 10 or 12 repeat units give rise to tubular assemblies with internal diameters of 10 and 13 Å, respectively [114, 115]. When the periphery is rendered hydrophobic, such tubular aggregates can be inserted into lipid bilayers to create transmembrane channels [116]. For example, channels consisting of *cyclo*-[-(L-Trp-D-Leu)<sub>n</sub>-L-Glu-D-Leu-] with  $n=3$  possessing an inner diameter of 7 Å show transport activity for potassium and sodium ions close to that of the natural gramicidin A. Increasing the inner channel diameter to 10 Å by using an extended cyclopeptide with  $n=4$  leads to glucose transport activity [114]. This remarkable selectivity is based solely on pore size and points to potential applications in controlled drug delivery. Finally, the inner pore could recently be rendered hydrophobic by incorporating triazole-containing  $\epsilon$ -amino acids [117].

Seebach et al. have found that the cyclic tetramers of 3-aminobutanoic acid 32–34 (Fig. 26) adopt tubular structures in a fashion similar to those of  $\alpha$ -peptides described earlier [118]. X-ray powder diffraction data suggest that all three  $\beta^3$ -peptide isomers exhibit tubular crystal packing with non-linear H-bonding. Presumably, the additional methylene group provides the rings with more flexibility and allows them to adopt a conformation suitable for stacking.

Homochiral cyclic  $\beta^3$ -peptides such as *cyclo*-[-( $\beta^3$ -Htrp)<sub>4</sub>-] are able to form transmembrane ion channels with pore sizes of 2.6–2.7 Å [119, 120]. The nanotubes contain a parallel  $\beta$ -sheet-like structure in contrast to their alternating  $\alpha$ -peptide counterparts described above. The parallel arrangement of amide

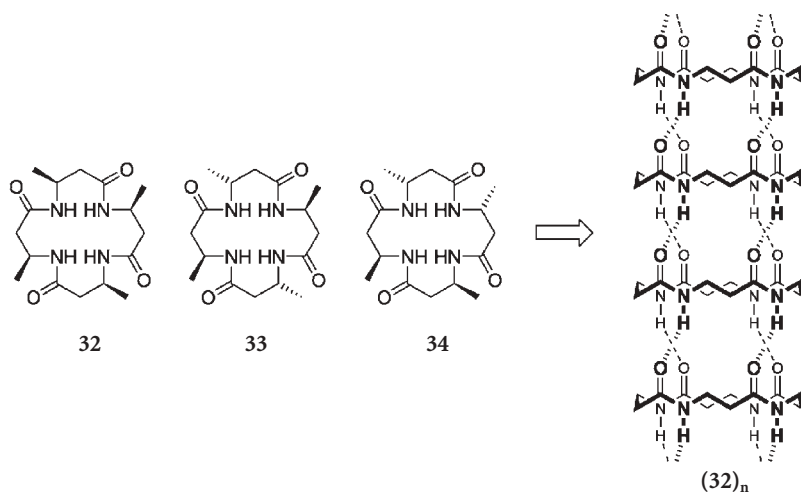


**Fig. 26** Seebach's cyclic  $\beta$ -peptide tetramers 32–34 and mode of self-association for 32 (side chains are omitted for clarity)

units causes formation of a net dipole in the resulting nanotube, which might affect channel conductance by voltage gating and display current rectification behavior.

The use of spirobicyclic peptides affords tubes that are covalently linked. This has been demonstrated by Ranganathan et al. who synthesized cystinospirane cycle 35, which displays a stacked tubular structure due to progressing H-bonding interactions in the crystal (Fig. 27) [121].

Serinophanes, which belong to the class of cyclodepsipeptides and contain alternating repeats of serine and aromatic units in the cyclic framework, have

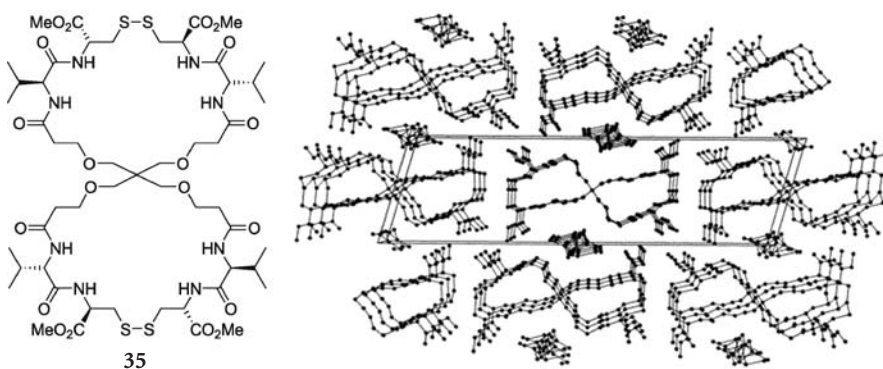


**Fig. 27** Ranganathan's fused tubes from spirobicyclic peptide 35. Reproduced in part with permission from reference[121]

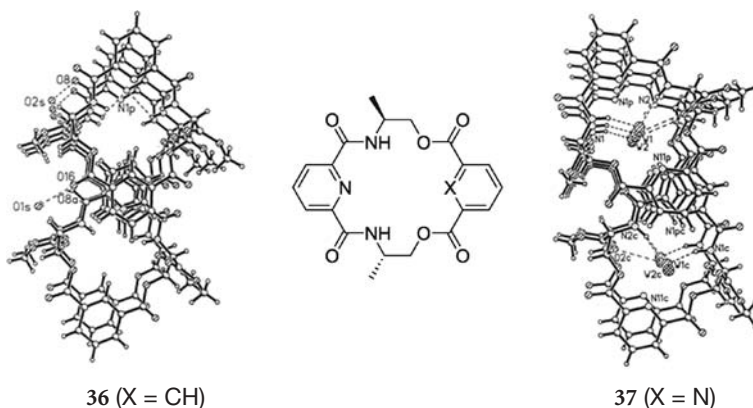


**Fig. 28** Serinophanes **36** and **37** forming different types of channels in the solid state. Reproduced in part with permission from reference [122]

been shown to generate tubular assemblies (Fig. 28) [122]. In this case, H-bonding is used for conformational stabilization in an intramolecular fashion only, while intermolecular  $\pi,\pi$ -stacking is responsible for the preferred tubular packing arrangement. Both macrocycles **36** and **37** form stacks with interdigitating aromatic units. In contrast to **37**, retained water molecules in **36** cannot be accommodated inside the tubes due to steric crowding of internal benzene protons, and are located in between sheets instead.

Tubes with an inner diameter of 3 Å have been obtained from an 18-membered lactam, i.e., *cyclo*-(NHCH<sub>2</sub>CH=CHCH<sub>2</sub>CO)<sub>3</sub> [123]. The dipolar anisotropy arising from the same orientation of the amide groups amounts to a strong dipole along the tubular axis, which is amplified in the bulk to give a highly anisotropic crystalline material. Macrocyclic bisureas and bisamides, so called hybrid cyclopeptides, have been explored by Ranganathan [124]. Their tubular stacking in the solid state reveals the expected intermolecular H-bonding interactions between individual rings.

### 5.1.2

#### Cyclic Oligosaccharides

Cyclic oligosaccharides **38**, having alternating (1→4)-linked  $\alpha$ -D- and  $\alpha$ -L-rhamnopyranose residues, and **39**, having alternating (1→4)-linked  $\alpha$ -L-rhamnopyranose and mannopyranose residues, have been described by Stoddart and coworkers (Fig. 29) [125–127]. X-ray crystallography shows that the cycles stack in a head-to-tail fashion to form tubular channels with inner diameters of ~10 Å. Interestingly, intermolecular H-bonds do not stabilize the individual stacks along their tubular axis but rather connect adjacent columns.

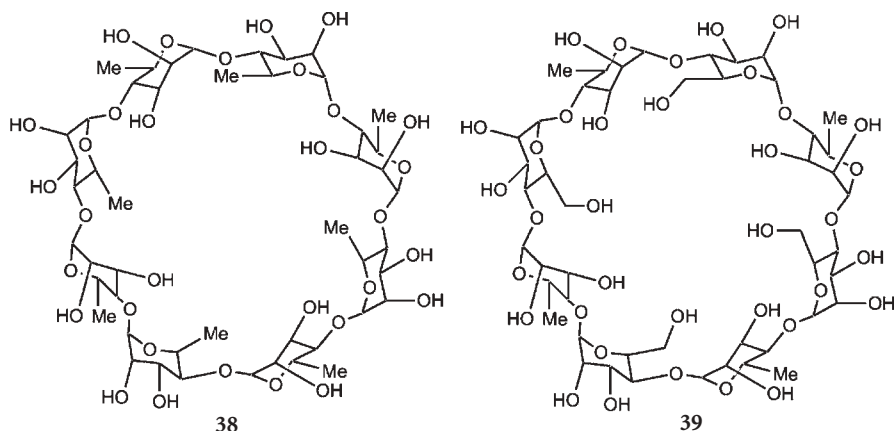


**Fig. 29** Stoddart's stacked cyclic oligosaccharides 38 and 39

### 5.1.3

#### Phenylene Macrocycles

A variety of phenylene-based macrocycles have been synthesized and crystallographically characterized by Schlüter's group [111, 128]. While most macrocycles crystallize in an "interpenetrating" manner, thereby avoiding channel formation, one example of a tubular stacking mode has been described [129]. The giant macrocycle **40** has been shown to adopt a cyclohexane-type chair conformation (Fig. 30). In the crystalline lattice, these chairs stack in such way that the inner cavity is continued, to give rise to a tubular structure having a huge internal diameter of  $\sim 27$  Å. These large inner cavities are most likely filled with solvent ( $\text{CHCl}_3$ ).

### 5.1.4

#### Phenylene Ethynylene Macrocycles

Moore and coworkers have been utilizing *meta*-connected phenylacetylenes, not only for creating a foldamer family (see 3.4) but also a variety of macrocycles (and dendritic architectures) [110, 130, 131]. For example, they reported the crystal structure of macrocycle **41** (Fig. 31), carrying peripheral phenolic groups [132]. In the solid state, hexagonally close-packed, two-dimensional H-bonded networks form layers that stack while approximately maintaining the alignment between the internal voids to afford extended channels with diameters of  $\sim 9$  Å (Fig. 32). In analogy to graphite, the sheets are separated by 3.33 Å and are arranged in a repeating ..ABCABC.. sequence of cubic close packing.

Macrocycles functionalized with bulky peripheral *t*-butyl groups show different organizations in the crystalline lattice depending on their internal sub-

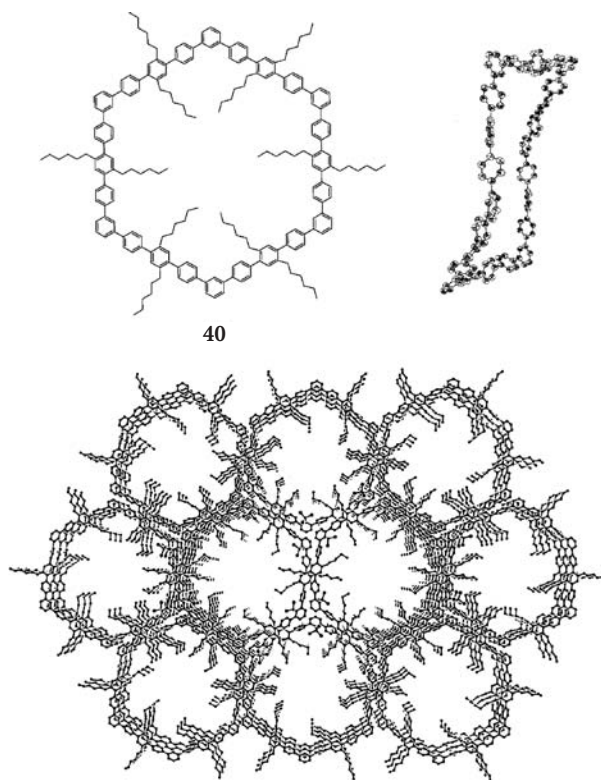


**Fig. 30** Schlüter's large phenylene macrocycle **40** and its crystal structure showing a chair-like conformation and columnar stacking to generate large inner channels. Reproduced in part with permission from reference [129]

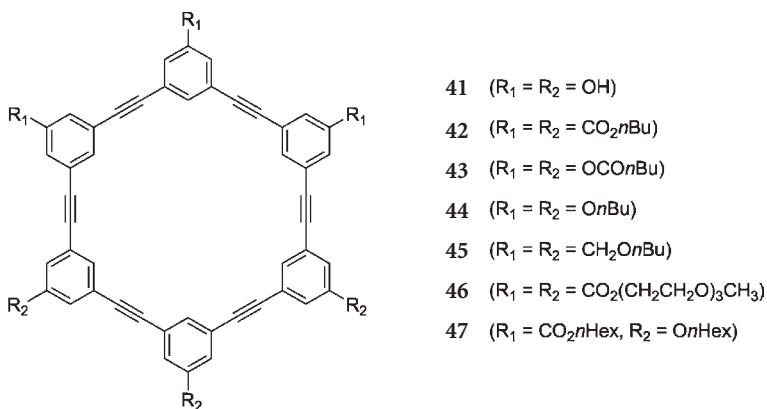


**Fig. 31** Several members of Moore's shape-persistent phenylene ethynylene macrocycles

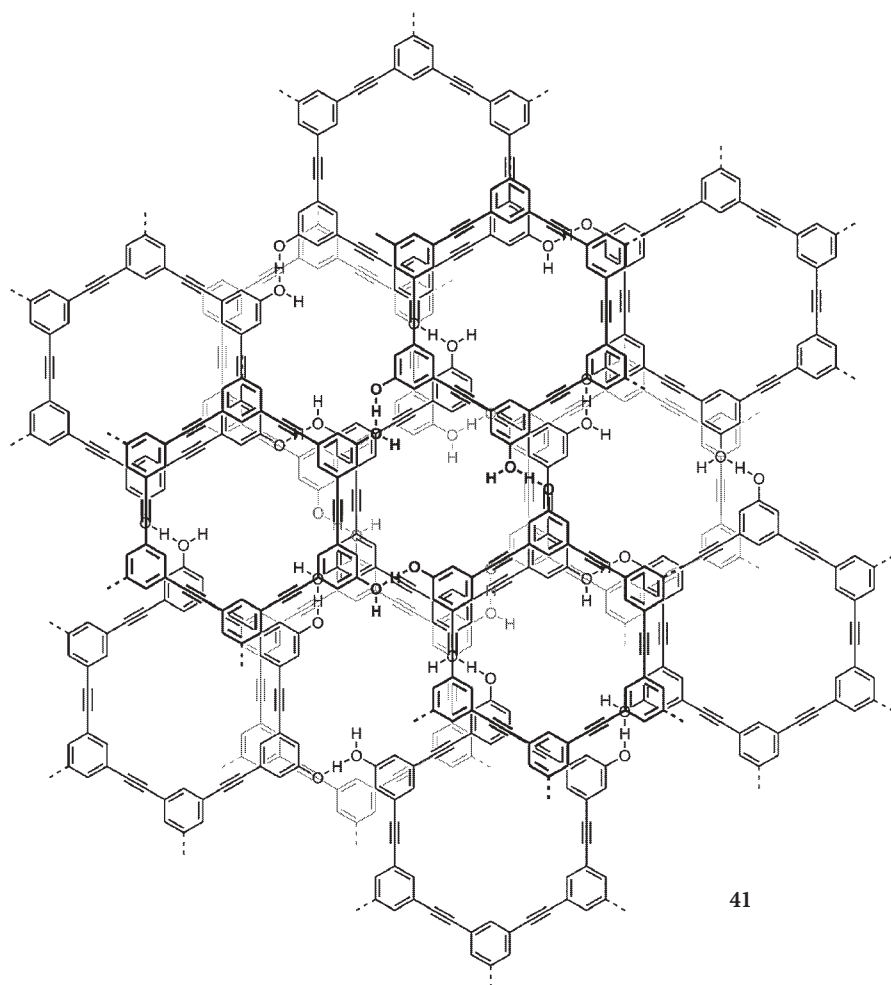


**Fig. 32** Arrangement of macrocycle **41** in the crystalline lattice yielding a mesoporous material

stitution pattern (Fig. 33). Bunz and coworkers reported macrocycle **48**, which does not form a truly tubular arrangement in the solid state due to a large tilt of the aromatic rings with respect to the column axis [133]. In contrast, the corresponding derivative **49** with internal methoxy-groups, described by Oda's group, exhibits the characteristic tubular packing arrangement, thereby generating open channels with pore sizes of 4.5 Å [134]. In this case, a 3.7 Å inter-sheet separation was found.

Solvent-triggered conformational change was observed for macrocycle **50** (Fig. 34) [135]. Crystallization from polar solvents such as pyridine resulted in a conformation where two phenolic and two hexyloxy groups occupy the inte-

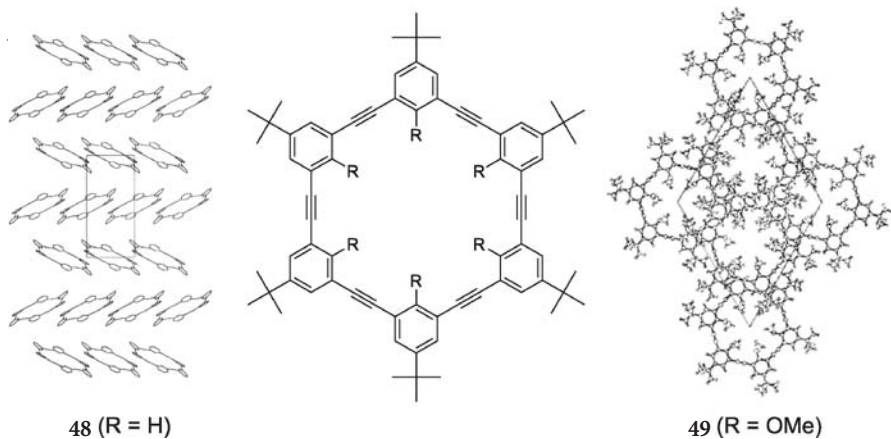


**Fig. 33** Bunz' and Oda's hexameric phenylene ethynylene macrocycles 48 and 49 show different packing behavior dependent on their internal substitution pattern. Reproduced in part with permission from references [133] and [134]

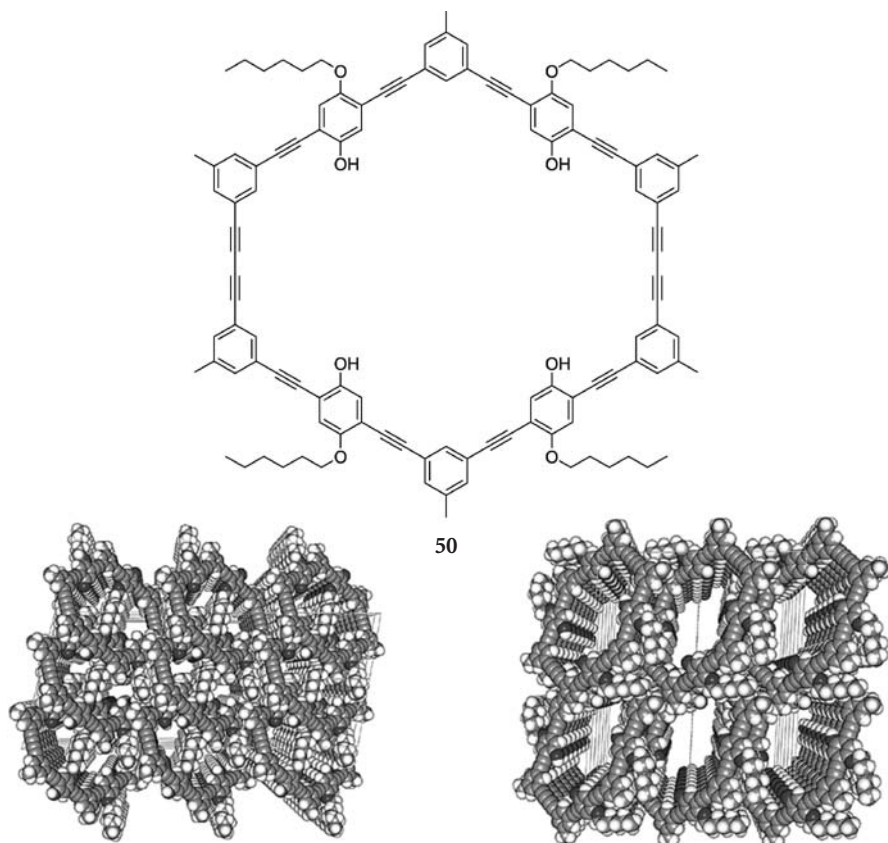


**Fig. 34** Höger's macrocycle 50 exhibits different aggregation modes in the solid state depending on the crystallizing conditions, by exposing and hiding different parts of its flexible amphiphilic substituents. Reproduced in part with permission from reference [135]

rior cavity leaving channels with a pore size of  $\sim 4\text{--}5$  Å. However, when the same macrocycle was crystallized from THF, a less polar solvent, all hexyloxy side chains were exposed to the outside and therefore a channel structure with much larger oval inner pores of  $8\times 12$  Å was obtained.

## 5.2

### Tubular Structures at Interfaces

The rigid macrocycles are able to form highly ordered monolayers at the air/water interface. In these compact monolayers, macrocycle **47** adopts an edge-on orientation with respect to the subphase while individual cycles stack to afford a tubular channel running parallel to the subphase normal, as shown by GIXD and XR [136]. The order in the layers can be either enhanced by addition of KCl or disrupted by adding CsCl. Assuming cation-binding to the cycle's periphery or side chains, it was speculated that the smaller potassium ions primarily provide additional stabilization to the aggregate, while the larger cesium ions predominantly hinder stacking due to their significant spatial requirements.

In related work, the self-assembly of *cyclo*-[-(L-Phe-D-N-MeAla)<sub>4</sub>-] at the air/water interface has been investigated [137]. Due to N-methylation blocking H-bonding interactions on one face of the cyclopeptide, only dimeric aggregates can be formed. With the help of GIXD, it was shown that three layers of peptide dimers adopt a face-on orientation with respect to the subphase. By changing the amino acid residues to yield *cyclo*-[-(L-Trp-D-Leu)<sub>3</sub>-L-Ser-D-Leu-], crystalline monolayers of nanotubes lying parallel to the water surface in an edge-on orientation were obtained. Interestingly, replacing the hydrophilic serine with another tryptophan residue affords a cyclopeptide that exhibits a very low tendency to form such ordered monolayers. This finding clearly demonstrates the dramatic effect of side chains substitution on peptide self-assembly at interfaces.

## 5.3

### Tubular Structures in Mesophases

Owing to the rigid frame work and side chains mobility, shape-persistent macrocycles can be envisaged as mesogens of a tubular mesomorphic state, in which the chemically defined interior of the formed channels provides the opportunity to create amendable porous materials. Zhang and Moore observed and characterized the tubular liquid crystalline (LC) mesophase of macrocycle **47** by optical microscopy, DSC, and powder X-ray diffraction [138]. Later on, the mesophase was doped with silver ions, which were intercalated within the tubes without destroying the LC order as shown by high-resolution X-ray diffraction [139]. This study illustrates the potential use of tubular LC phases from macrocycles for preparing optoelectronic materials.

Besides forming a mesophase, the macrocycle can also be organized within a LC phase. This has recently been demonstrated by Dory and coworkers, who utilized self-assembly of a lactam (see 5.1.1) in a nematic phase to generate aggregates of nanotubes having micrometer diameters and millimeter lengths [140].

## 5.4 Tubular Structures in Solution

### 5.4.1 Phenylene Ethynylene Macrocycles

As early as 1992, Zhang and Moore reported on the ability of macrocycle **42** to self-aggregate in solution at higher concentrations [141]. NMR titration experiments monitoring the up-field shift of aromatic protons with increasing concentration indicate cooperative  $\pi,\pi$ -stacking interactions between the aggregating macrocycles. Since then, a number of macrocycles have been studied and it was found that the self-association behavior varies with the structure of the backbone as well as the side chains [110]. In agreement with Hunter and Sanders [61, 62, 142], electron-poor aromatic systems such as benzoates in macrocycles **42** favor aggregation, while in the case of electron-rich moieties such as phenolates (**43**), phenyl ethers (**44**), and benzyl ethers (**45**), no self-association was found [141]. The association constants were deduced from NMR and VPO studies, which confirmed that no aggregates larger than dimeric were formed in chloroform. Later on, the same group introduced an additional solvophobic driving force by substitution with polar triglyme side chains (**46**) and as a result, higher association constants leading to formation of larger (than dimeric) aggregates were obtained [63]. Again, aggregation could be correlated to electronic requirements for  $\pi,\pi$ -stacking in analogy to the solvophobic driven helical structure formation in the related foldamer family (see 3.4). Surprisingly, the same macrocycle (**46**) also aggregates in benzene. The association constant can be further improved by internal methyl substitution [143], owing to reduction of void volume.

### 5.4.2 Phenylene Diethynylene Macrocycles

Similar to the *meta*-phenylene ethynylene macrocycles, Tobe et al. investigated the self-aggregation of a series of macrocycles having *meta*-phenylene diethynylene backbones (of different sizes) bearing polar or non-polar side chains [144]. Incorporation of the diacetylene linkage renders the aromatic rings more electron-deficient and therefore results in the higher self-association constants of **51** and **52** when compared to the corresponding *meta*-phenylene ethynylene macrocycles. Electrostatic repulsion among pyridine or cyano

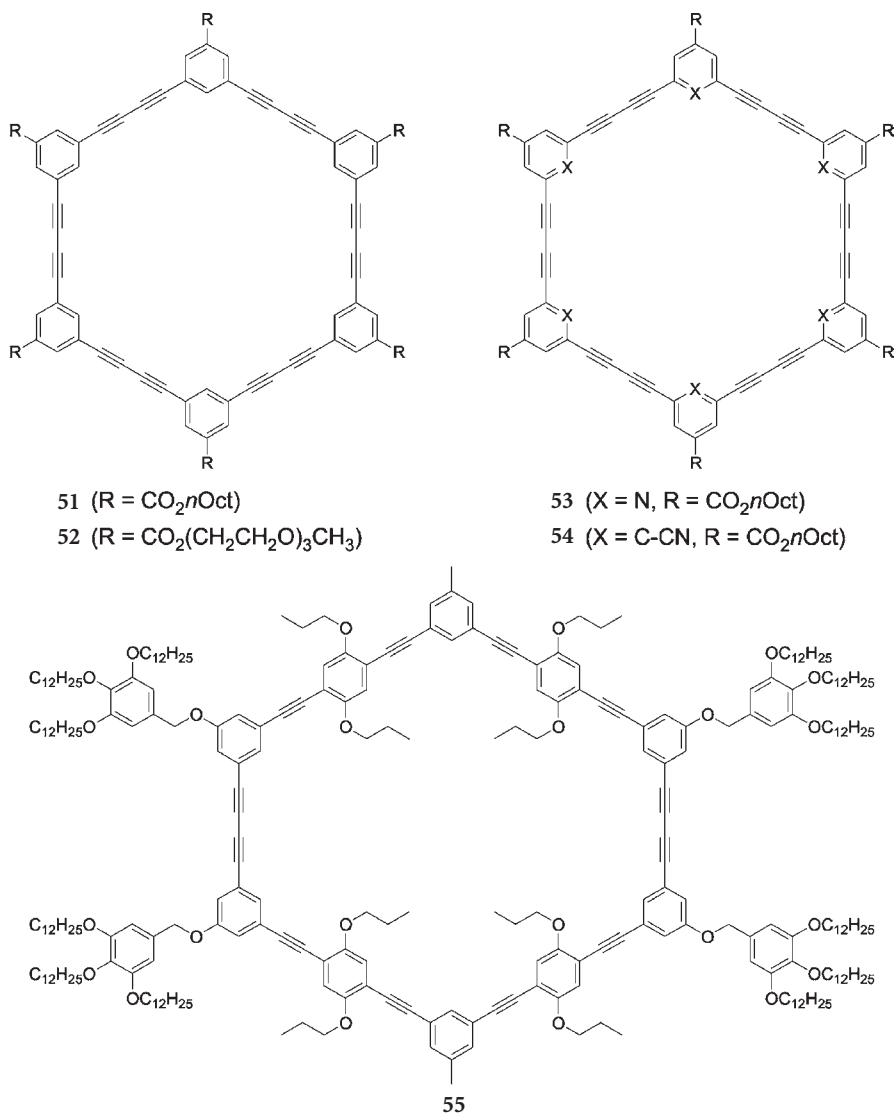


**Fig. 35** Tobe's phenylene diethynylene macrocycles 53 and 54 that do not self-associate but form columnar heteroaggregates with macrocycle 51. Höger's macrocycle 55, having an electron-rich aromatic backbone surrounded by a non-polar corona, self-aggregates in non-polar solvents

groups prohibits self-aggregation in the case of macrocycles 53 and 54, respectively (Fig. 35) [145, 146]. However, these compounds can form heteroaggregates with macrocycle 51, presumably driven by favorable dipolar interactions between the phenylene and electron-deficient benzonitrile/pyridine moieties.

Introduction of large hydrophobic substituents leads to reversal of amphiphilicity in macrocycle **55**, (Fig. 35) and hence self-association occurred at higher concentrations in non-polar solvent mixtures [147]. Interestingly, the rather electron-rich phenyl ether backbone units do not seem to interfere with aggregation.

### 5.4.3 Coil-Ring-Coil Block Copolymers

A remarkable study by Höger and coworkers describes the self-assembly of coil-ring-coil block copolymers **56**, in which the macrocycle is linked in between two narrow disperse polystyrene blocks of various lengths (Fig. 36) [148]. Upon cooling in cyclohexane, the stacking of the cyclic moieties driven by the amphiphilic structure results in formation of hollow cylinders with an average length of ~500 nm. A combination of DLS, X-ray scattering, TEM, and AFM experiments confirms the existence of such long cylindrical aggregates. The high persistence length of this supramolecular polymer of ~100 nm indicates the surprisingly high rigidity of the structure.

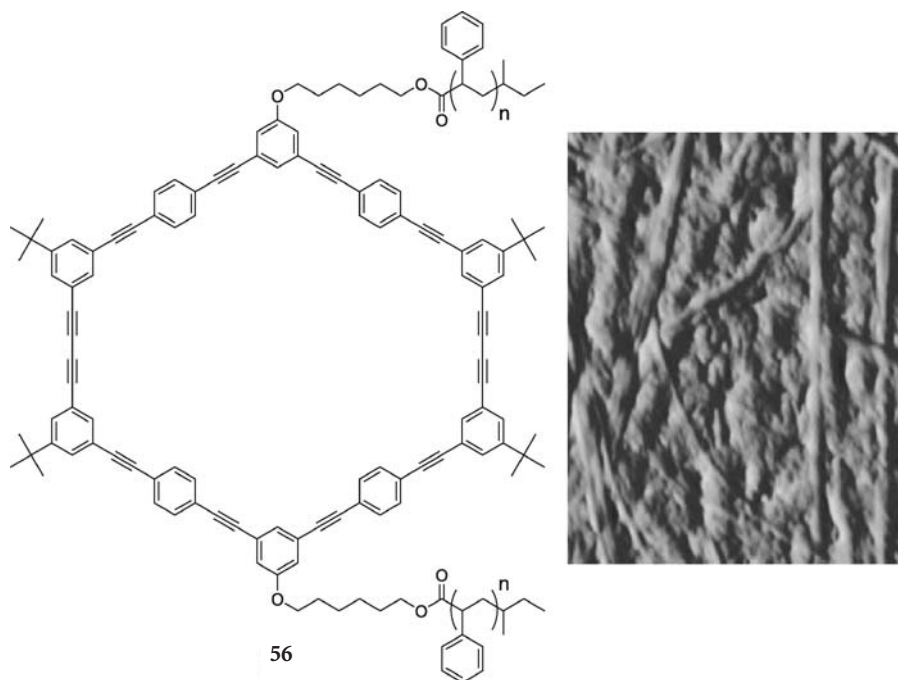


**Fig. 36** Höger's coil-ring-coil block copolymers **56** forming long aggregates of stacked rings surrounded by a polystyrene sheath. AFM image of 0.15 wt% **56** in cyclohexane on mica. Reproduced in part with permission from reference [148]

#### 5.4.4

#### Covalent Stabilization by Crosslinking

Although self-assembly utilizing various non-covalent interactions offers significant advantages such as minimization of synthetic efforts, high efficiency, assembly control via information-rich backbones among others, the resulting supramolecular structures often exhibit low kinetic stability due to rapid assembly-disassembly processes. Thus, covalently locked structures can be advantageous in view of certain future materials applications. In this section, the few related examples, where the target structure is formed by self-assembly of the subunits and then covalently captured, are discussed.

#### 5.4.5

#### Cyclodextrins

The well-known ability of cyclodextrins to form inclusion complexes with a wide range of guest molecules in aqueous solution due to their cylindrical

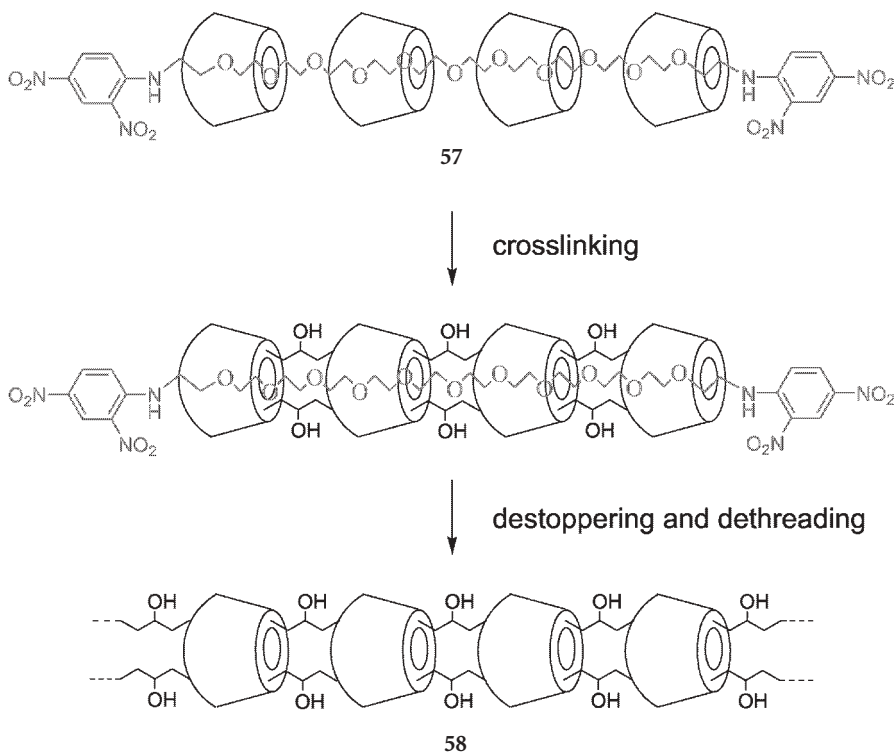


**Fig. 37** Harada's approach to cyclodextrin-based nanotubes **58** via formation, subsequent covalent crosslinking, and final template removal from polyrotaxane **57**

0.7 nm-deep cavities having diameters of 0.45, 0.7, and 0.85 nm for the  $\alpha$ -,  $\beta$ -, and  $\gamma$ -forms, respectively, has been exploited by many researchers for the construction of polyrotaxanes. In 1992, Harada et al. reported the threading of approximately 20 cyclodextrin molecules onto a diamino-terminated polyethylene glycol to afford a pseudopolyrotaxane, which was capped using Sanger's reagent to afford polyrotaxane **57** of lengths up to 20 nm (Fig. 37) [149]. Subsequent crosslinking involving the reaction of adjacent cyclodextrin hydroxyl groups with epichlorohydrin followed by removal of the polymeric template via de-stoppering and de-threading, yielded the desired macromolecular tubes **58** [150]. The tubes are soluble in water and polar organic solvents. In an analogous approach, Liu et al. prepared tubular dimers from  $\beta$ -cyclodextrin derivatives linked by selenium and platinum complexes [151].

#### 5.4.6

##### Cored Dendronized Polymers

In order to extend their unimolecular imprinting concept [152] from cored spherical dendrimers [153] to a cylindrical topology, Zimmerman and coworkers realized a three-step sequence of assembly, crosslinking, and core removal [154]. This approach is related to Harada's synthesis of cyclodextrin nanotubes (see 5.5.1); however, the crosslinking step occurs in an intramolecular rather than an intermolecular fashion. Tin porphyrin **59**, carrying four polybenzylether dendrons attached via ester moieties and containing multiple olefin terminal groups, represents the key building block of the synthesis (Fig. 38). Addition of succinic acid serving as bridging ligand yields relatively unstable coordination oligomers with, on average, five face-to-face-oriented tin porphyrin repeat units. Subsequent RCM of the peripheral olefin groups leads to an extensively crosslinked periphery with low degrees of interoligomer crosslinking at high dilution. Finally, the internal porphyrin core was removed using transesterification of the internal ester linkages.

#### 5.4.7

##### Cyclic Alternating D,L- $\alpha$ -Peptides

Taking advantage of the well-defined H-bonding pattern in stacking cyclic peptides (see 5.1.1), Ghadiri and coworkers have successfully captured the preorganized dimeric peptide assemblies by intermolecular covalent bond formation (Fig. 39). In both cases, association was restricted to one face of the cyclic peptide by means of N-methylation (*vide supra*). Specifically, olefin-containing *cyclo*[-(L-Phe-D-N-MeAla-L-Hag-D-N-MeAla)<sub>2</sub>-] **60** undergoes regioselective intermolecular RCM to afford covalently stabilized  $\beta$ -sheet peptide dimer **62** [155]. In another example, the dimeric complex of *cyclo*[-(L-Phe-D-N-MeAla-L-Cys(Acm)-D-N-MeAla)<sub>2</sub>-] **61** was locked by oxidative disulfide formation [156]. So far, this promising approach has been limited to covalent stabilization of dimeric aggregates only.

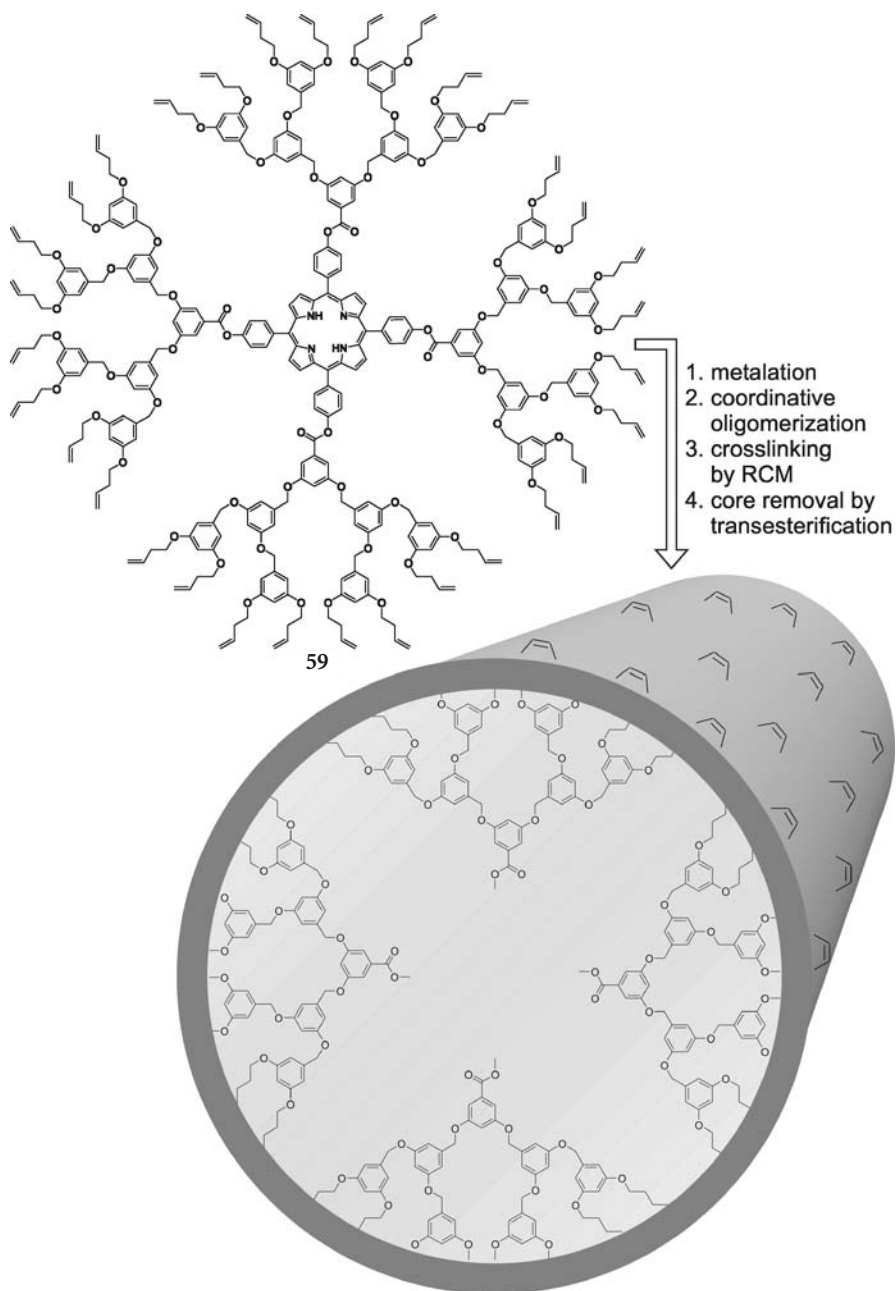


**Fig. 38** Zimmerman's approach to organic nanotubes via cored dendronized polymers based on **59**

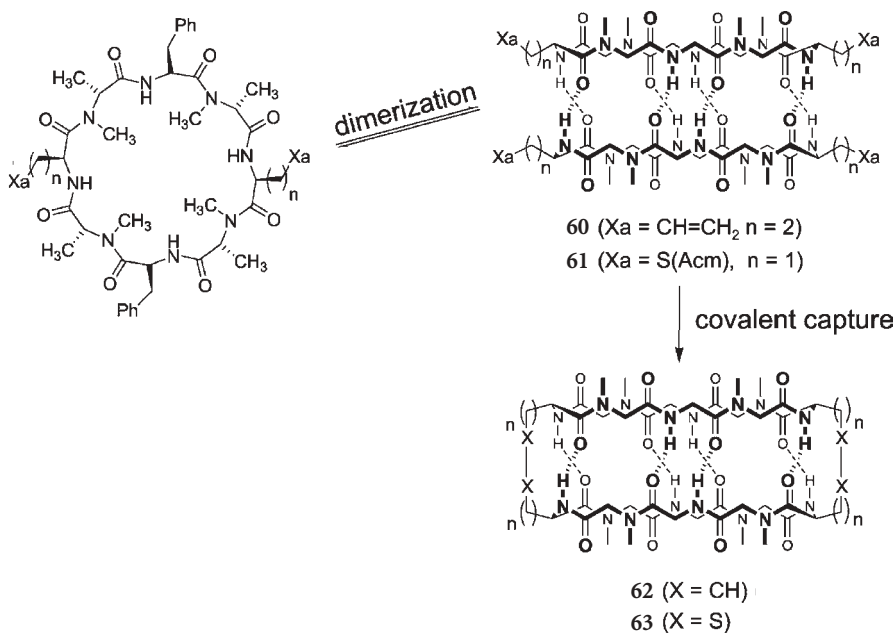


**Fig. 39** Ghadiri's covalent capture of defined cyclopeptide dimers **60** and **61** using RCM or disulfide formation. Reproduced in part with permission from reference [156]

## 6 Tubes from Stacked Rosettes

The degree of sophistication can be increased by orthogonal self-assembly, which uses non-covalent interactions not only for stacking along the tubular axis, but also to create the cyclic cross-sections themselves. These self-assembled mimics of the covalent macrocycles covered in the previous section are frequently referred to as rosettes. In order to take advantage of the 3D organization of small molecular building blocks into defined complex supramolecular structures, a detailed understanding of the principles of self-assembly and its key interactions is required [4, 7]. In the context of this section, H-bonding and aromatic  $\pi$ - $\pi$ -stacking interactions as well as solvophobic and electrostatic effects are of particular importance. In particular, the H-bond is a common motif found in Nature and has been extensively explored for the generation of artificial rosette-like structures. The overview given in this section covers two important rosette families, focusing on assemblies in solution and liquid crystals. Related structures that are only known in the solid state [157] as well as coordination assemblies incorporating metal ions in the tube walls have been omitted [158].

## 6.1

## G-Quartets and Related Motifs

One of the most studied examples of artificial rosettes involves guanine **64**, which is known to form tetrameric self-assembled disk-like structures, so-called G-quartets, around metal ions in water as well as in the LC solid states. Multiple H-bonds between the guanine units and additional metal coordination to the templating cations in the central cavity (0.45 nm diameter) render the assembly remarkably stable (Fig. 40) [159]. Lipophilic analogs, such as bis-decanoyl-deoxyguanosine **65** investigated by Gottarelli and coworkers, also assemble in organic solvents, taking advantage of the solvophobic effect (*vide supra*). The addition of alkaline ions (1/8 eq.) promotes stacking of these G-quartets into discrete octameric sandwich-like complexes with the metal coordinated to eight carbonyl-oxygens [160, 161]. Upon further addition of cations, the G-quartets continue to stack to form columnar polymeric aggregates. These supramolecular ion channels possess a stoichiometry of guanine:cation=4:1 [162]. The introduction of bulky substituents in the 8-position, as in compound **66**, even allows assembly into stable quartets without the need

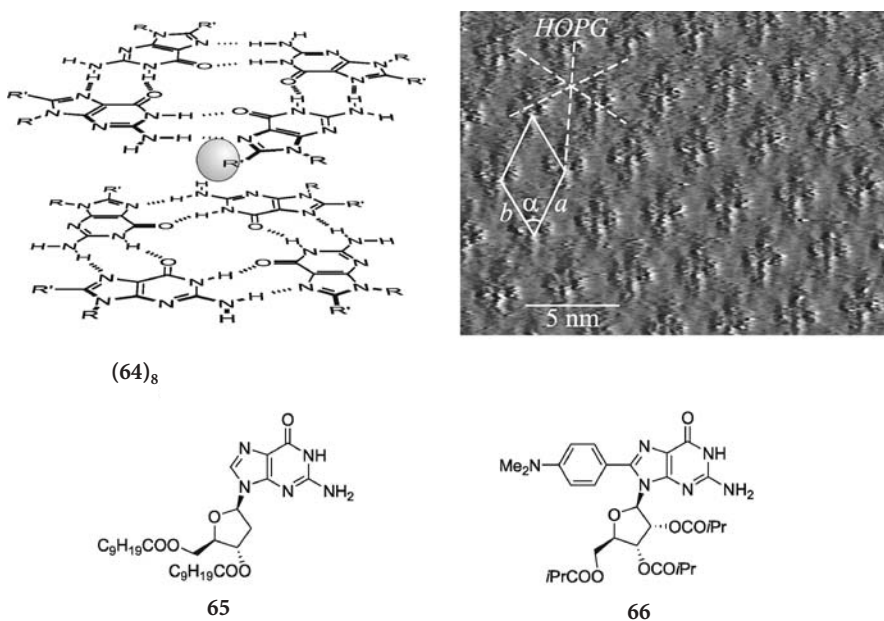


**Fig. 40** Gottarelli's and Sessler's G-quartets based on guanine **64**. The first step towards columnar stacks is represented by two G-quartets intercalated by a potassium ion. The STM image shows a hexagonal array of 8-oxoguanosine G-quartets at the solid-liquid interface. Amphiphilic guanosine derivative **65** displaying solvophobicity-assisted assembly and bulky guanosine derivative **66** that assembles without cation mediation. Reproduced in part with permission from [164]. HOPG Highly ordered pyrolytic graphite

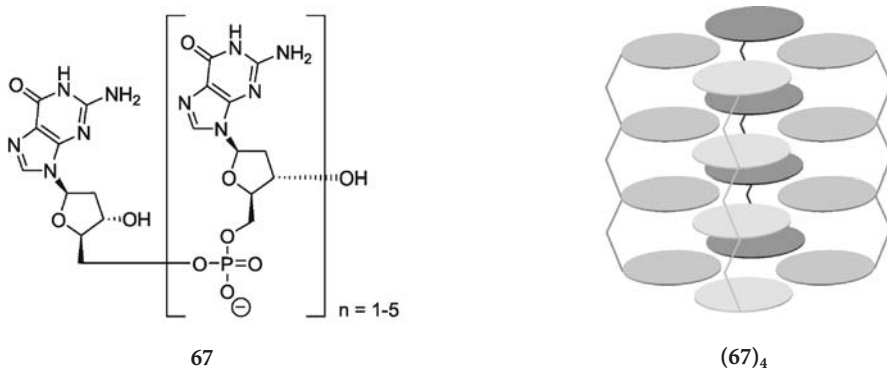


**Fig. 41** Oligoguanosine **67** and cartoon of barrel-forming oligoguanosine **67** tetramer

of templating cations, whereas other assembling motifs become sterically unfavorable, as shown by Sessler [163]. Oxyguanosine derivatives that assemble in the absence of cations into tubular helical arrays in similar fashion as stacked G-quartets have also been reported recently [164].

Oligomers of deoxyguanosine phosphate also self-organize into columnar stacks forming LC phases. Deoxyguanosine oligomers **67** (dimer to hexamer) were shown to assemble into discrete tetrameric barrels, which can stack to afford columnar nanoobjects (Fig. 41) [165].

The guanine self-organization properties were exploited to assemble supramolecular tubes of calixarenes [166]. Here, the repeating unit is a calix[4]arene with four guanosine moieties attached to it in a 1,3-alternating fashion. The addition of cations triggered the assembly of G-quartets arranging their parent calix[4]arenes into ordered columns in a highly cooperative way.

Isoguanosines form even stronger G-quartets than guanine-based systems and they also display cation-mediated sandwich-type octamer formation [167]. However, in this case the resulting assemblies are not planar and thus columns cannot be obtained. Interestingly, cesium cations are capable of templating expanded pentameric discs that dimerize to sandwich-type complexes [168]. In the presence of photoreactive thymidine residues in synthetic DNA strands, such discotic pentamers could successfully be crosslinked by [2+2] photodimerization [169].

Retaining the double H-bonding motif of guanine and expanding its five-membered heterocycle to the homologue six-membered ring yields the pterine heterobicyclic system. In analogy to the guanine-based systems, folate **68** (Fig. 42) assembles into tetrameric planar discs that pile to form columns in solution as well as in the LC and solid phases [170]. In solution, the column length can be tuned by changing concentration and temperature as well as by adding salts, thereby yielding a maximum average length of 8.5 nm corresponding to about 25 piled discs. The column radii are around 1.45 nm and their inner voids

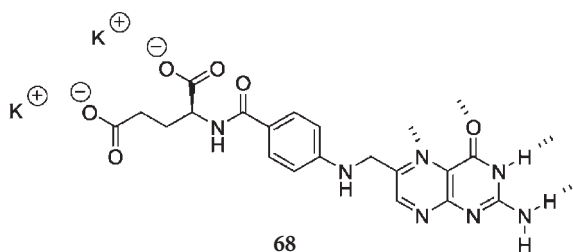


**Fig. 42** Gottarelli's folate **68** as a guanine analogue with same array of H-bond-donors and acceptors and therefore displaying G-quartet formation and stacking

can host potassium and sodium ions as well as water molecules [171]. In related approaches, Zimmerman et al. extended the heteroannulene feature to pyridoquinoline [172] and 1,8,9-triazaanthracene [173] derivatives that assemble in solution via multiple H-bonding interactions to form either stable trimers or hexamers; however, no stacking of these rosettes has been reported.

## 6.2

### Melamine–Cyanuric Acid Motifs

The cyclic melamine–cyanuric acid H-bonding motif was introduced by Whitesides and coworkers and intensively applied to the construction of supramolecular rods of stacked rosette-like assemblies with inner diameters of 5.9 Å [174]. Alternative assembly modes giving rise to ill-defined linear aggregates were excluded by controlling the steric crowding at the periphery of the subunits. Using complementary building blocks of tongs-shaped bisisocyanurates **69** and bismelamines **70**, self-assembled cylinders with a diameter of 5 nm are spontaneously formed in organic solvents [175]. Further aggregation yields the corresponding cylinder bundles with lengths up to 1.5 μm (3,000 stacked rosettes). The design takes advantage of solvophobicity driven, H-bonding-directed self-assembly between complementary tongs affording supramolecular rosettes that are covalently linked in a face-to-face fashion by the tongs' spacers (Fig. 43). An important feature involves the use of different spacer lengths in both complementary tongs in order to rule out a cage-type assembly. The same design concept was used by Timmerman, Reinhoudt et al. for generating similar nanostructures of orthogonal calix[4]arene dimelamine and calix[4]arene dicyanurate building blocks [176].

By replacing the cyanuric acid with an elongated and linear building block such as naphthalenedicarboximide, a rosette with enlarged dimensions can be obtained as shown by the work of Kunitake (Fig. 44, top) et al. [177]. The assembly of amphiphilic dialkylmelamine **71** with the complementary diimide **72** leads to the formation of columns that can further aggregate to yield fibers of micrometer length. Whether the individual columns having inner and outer diameters of 4 and 8 nm, respectively, consist of stacked rosettes or helical tapes

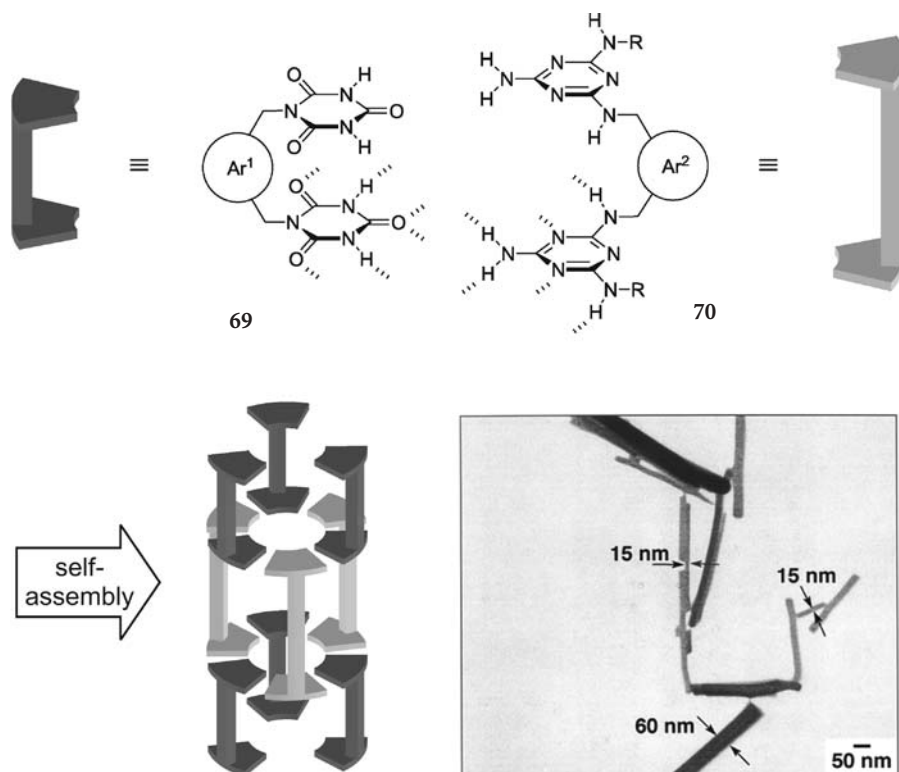


**Fig. 43** Whitesides' and Reinhoudt's approaches to stacked rosettes based on the melamine-cyanuric acid cyclic H-bonding array. Tong-shaped building blocks **69** and **70** co-assemble into cage-like substructures forming tubular stacks (Ar<sup>1</sup>, Ar<sup>2</sup>=benzene, furane, naphthalene, calix[4]arene). *Bottom right* is a TEM image of bundled aggregates formed from tubular assemblies. Reproduced in part with permission from [175]

remains unclear. In non-polar solvents, structure formation is driven by solvophobic as well as aromatic  $\pi,\pi$ -stacking interactions and directed by the H-bonding array.

Fenniri and coworkers designed a self-complementary heteroaromatic system **73** containing guanine and cytosine H-bonding arrays [178]. The relative orientation of the orthogonal binding sites leads to formation of hexagonal rosettes with an inner diameter of 1 nm (Fig. 44, bottom). By attaching chiral side chains at the periphery, supramolecular chirality was induced in the columns consisting of stacked rosettes [179]. Tuning and switching of chirality could be realized by binding chiral analytes to crown ethers covalently attached to the rosette's periphery.

Very recently, Meijer and coworkers reported on self-assembled nanotubes in solution consisting of chiral stacks of  $\pi$ -conjugated rosettes [180]. Wedge-shaped non-polar oligo(*para*-phenylenevinylene)s **74** and **75** having a di-

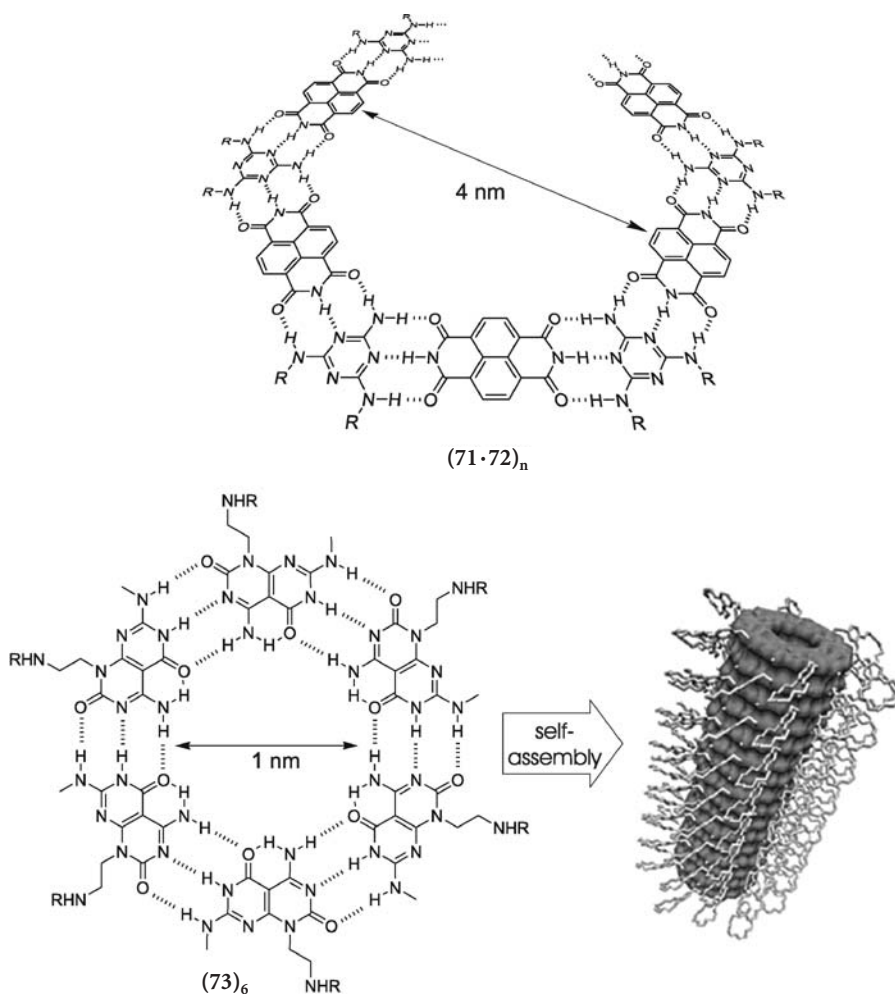


**Fig. 44** Kunitake's binary melamine-diimide system assembling to hollow cylinders via cyclic or helical assembling modes (*top*). Fenniri's rosette-forming pyrimido-pyrimidione 73, and 3D model of nanotube consisting of piled rosettes (*bottom*). Reproduced in part with permission from [179]

aminotriazine head group are able to form chiral cyclic hexamers with an inner void of 7 Å as visualized by STM (Fig. 45). Subsequent aggregation of the rosette subunits in non-polar solvents yields columns with lengths exceeding 185 nm in solution and 10 μm when cast on a solid substrate.

Finally, the classical H-bonding carboxylic acid dimer motif has been exploited by Hamilton and coworkers, who demonstrated the cyclic assembly of various isophthalic acid derivatives. Depending on the bulky substituent in the *meta*-position, individual or stacked rosettes were obtained in solution and in the crystal, respectively [181].

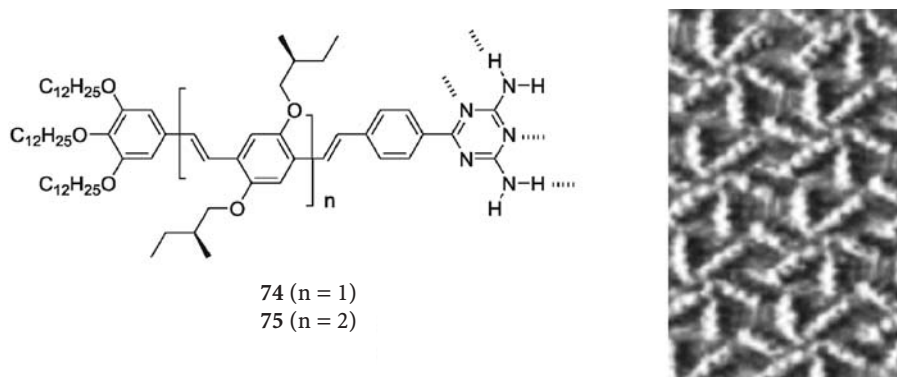


**Fig. 45** Meijer's oligo(*para*-phenylenevinylene)s capable of assembling into rosettes and subsequently into tubes. STM image of 75 shows a monolayer of chiral hexameric rosettes. Reproduced in part with permission from [180]

## 7

### Tubes from Self-Assembled Amphiphiles

Ultimately, directed non-covalent interactions and molecular rigidity/geometric constraints can be removed from the self-assembling building blocks. The resulting systems organize into higher aggregates based on their amphiphilicity and the proportions, i. e., aspect ratio, of their individual components [182]. In Nature, most cylindrical structures are not entirely founded on segregation of immiscible or solvophilic/solvophobic components but involve additional interactions. The tobacco mosaic virus (TMV) represents perhaps the most impressive and best illustration of this design concept [183]. In this case, the self-assembly of taper-shaped protein building blocks templated by viral RNA affords a cylindrical structure of controlled length, in which the subunits are held together by various non-covalent bonds. Artificial systems have been thoroughly investigated in an attempt to relate the different observed aggregation modes in solution, in the LC state, and in bulk to the amphiphile's structure. Components can vary from simple detergents [184] to complex (bio)macromolecular amphiphiles and block copolymers [185, 186]. In this section, three tubular design concepts are discussed in relations to the shape of the amphiphile. Emphasis is mostly put on the solution and LC phases.

#### 7.1

##### Wedge-Shaped Amphiphiles

Most common biological amphiphiles are lipids composed of long hydrocarbon tails and polar and/or ionic head groups. The aspect ratio of these building blocks, as well as their miscibility properties, defines the assembly structure [182]. The more pronounced the volume difference of head to tail becomes, the more curvature is introduced, and the more cyclic structures are realized.

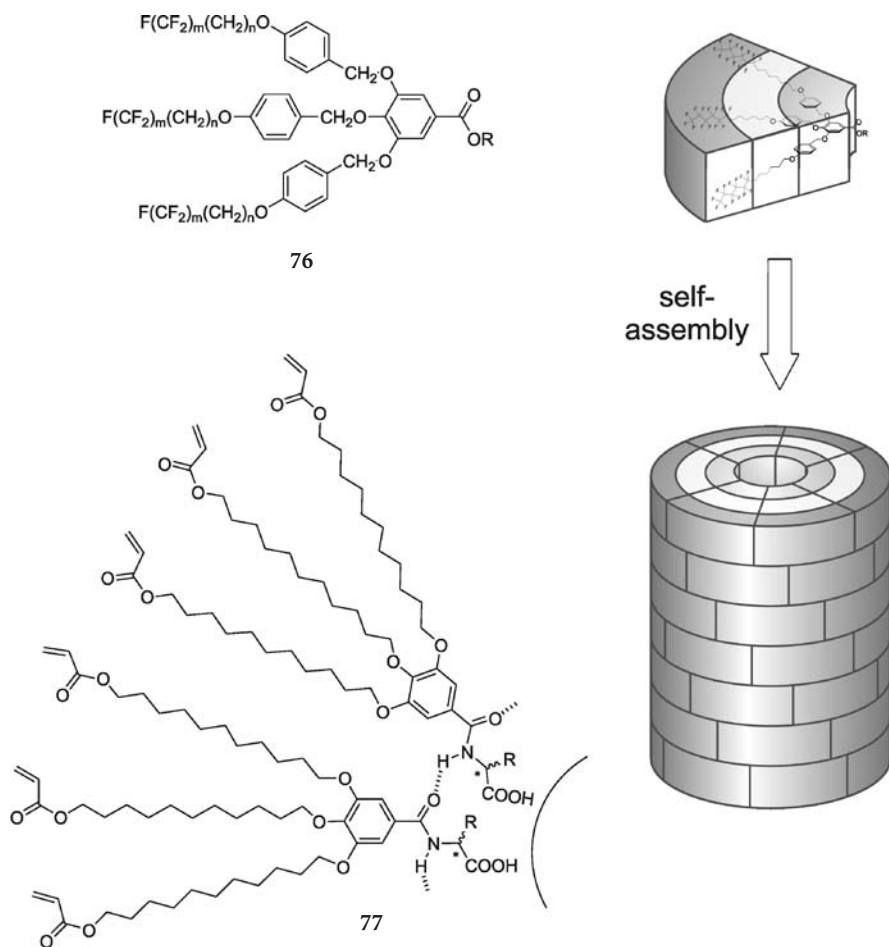


**Fig. 46** Percec's wedge-shaped amphiphilic gallate **76** (top), cartoon illustrating assembly of amphiphile into layered tubes; Gin's analogue gallate **77** with H-bond-stabilized inner core and crosslinkable periphery (bottom)

Wedge-, taper-, or sector-shaped amphiphiles can readily form cylindrical shapes in solution or suspension and inverted hexagonal phases with tubular channels in the LC state. Polar head groups form the inner periphery of tubes with the central channel filled with polar solvent molecules, while the disordered non-polar tails form the outer periphery and isolate the tubes from each other. Inspired by the structural organization found in TMV, Percec and his group designed flat taper-shaped dendritic amphiphiles **76**, based on gallic acid, which form five- to six-membered discotic assemblies, which further stack into columns in solution and their corresponding columnar LC phase (Fig. 46, top) [187]. The carboxylic acid function, which can also be esterified or ionized, serves as the hydrophilic head at the interior of the assembly, whereas long

linear chains, i. e., hydrocarbons or fluorocarbons, attached to a small aromatic branching unit generate bulkiness and hydrophobicity at the exterior. While the first systems only assembled via ion-mediated complexation processes [188, 189], wedge-shaped amphiphiles with semifluorinated tails also assemble solely via the fluorophobic effect [190]. In this case, the segregation of flexible perfluorinated and perhydrogenated segments forms a deformable sheath of onion-like layers within the cylindrical assembly with a rigid aromatic interior surrounding the hollow core. Upon casting on a surface, the columns further arrange into an inverted hexagonal LC phase with infinite column lengths and total column diameters reaching 6 nm [191]. Several approaches were shown to stabilize these structures. When the inner carboxylic acid functions are esterified with ion receptors such as crown ethers or ethylene glycols, lithium or sodium ions can template the self-assembly [192]. In an intriguing report, the same group recently demonstrated the packing of organic conducting units within the tubular cavity to create insulated molecular wires via this self-assembly strategy [193]. In another case, the interior has been functionalized with polymerizable groups and subsequent polymerization has led to covalent stabilization of the tubular assembly at the cost of inner void volume [194].

Gin and coworkers designed analogous taper-shaped gallic acid salt monomers with polymerizable olefin, diolefin, or acrylate units at the periphery of the hydrophobic tails allowing for crosslinking the inverted hexagonal LC phase without affecting the column's inner void [195]. Introduction of H-bond motifs, as in compound 77, further stabilized the columnar phases (Fig. 46, bottom) [196]. By the introduction of functional units such as emitting polymers or catalytically active sites, ordered nanocomposite materials have been obtained [195].

A similar crosslinkable amphiphile forming an inverted hexagonal LC phase was recently designed by Kim and coworkers [197]. The wedge-shape is realized by a polar G-2 amide dendron with a focal carboxylic acid group. Peripheral, linear hydrocarbon chains with incorporated diyne moieties control the segregation behavior of these molecules and allow for subsequent topochemical crosslinking.

## 7.2

### Linear Amphiphiles and Block Copolymers

A radical simplification of the design of tubular structures is achieved by the use of linear amphiphiles. The ease of their synthesis and frequently commercial availability is generally counterbalanced by the limited predictability of the self-assembling process due to the high flexibility and ill-defined shape of the building blocks. Two principal aggregation modes that lead to tubular architectures involve rolled lamellar sheets and cylindrical micelles. Formation of helical fibers, coiled ribbons, and tubules is a common motif in the assembly of lamellar sheets among lipids, with changes in concentration, solvent, temperature, and addition of salts being common stimuli to induce the formation

of desired structural features. The various formed architectures can be covalently stabilized by means of a crosslinking polymerization within the assembly [198, 199]. In view of their simple and large-scale preparation, such self-assembled nanotubes represent interesting candidates for potential applications in the life and materials sciences [200, 201].

Common amphiphile structures include: bolaamphiphiles [202], N-acylated amino acids [203], nucleic acid derivatives [204], double-chain ammonium salts **78** [205], unsaturated double-chain phosphatidylethanolamines **80** [206] and related diacetylenic phosphatidylcholines [207], (fluorinated) anionic glucophospholipids [208], and aldonamides or gluconamides [209, 210] (Fig. 47). Polymerizable diacetylenic aldonamides **82** assemble to structures of helical, tightly coiled bilayer sheets forming hollow and open-ended tubes (Fig. 47, bottom). Depending on the exact position of the diacetylenic function and the assembling conditions, tubes having lengths of several micrometers, as well as average inner and outer diameters of 8–10 nm and 50–70 nm, respectively, have been prepared [211]. In one case, outer diameters of up to 300 nm have been

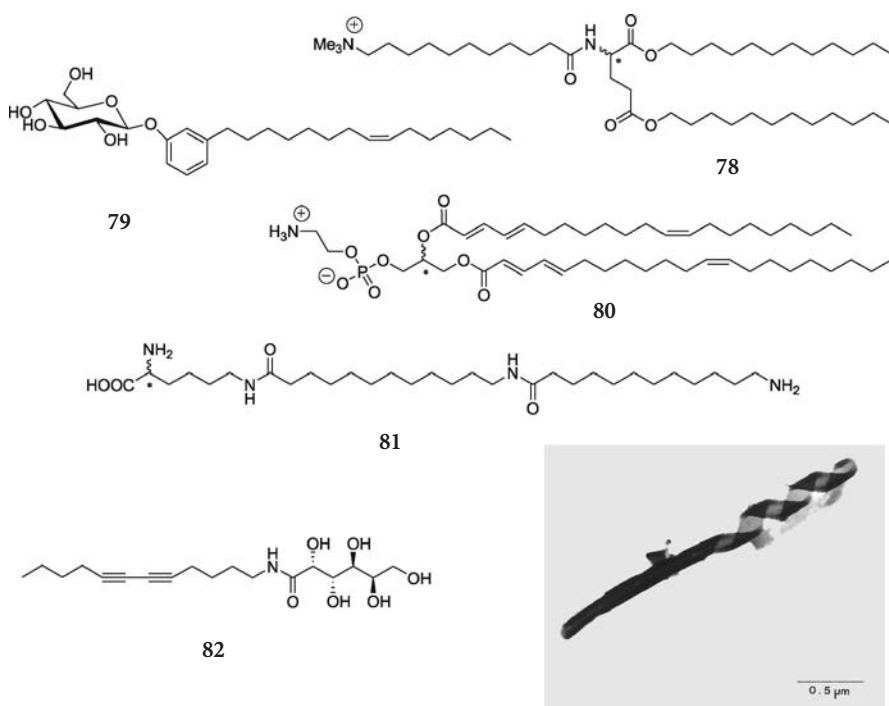


**Fig. 47** Selected linear amphiphiles assembling into tubes (*top*): double-chain ammonium amphiphile (**78**), aromatic glycolipid (**79**), unsaturated double-chain phosphatidylethanolamine (**80**), H-bond enhanced bolaamphiphile (**81**); diacetylenic aldonamide (**82**) and TEM of polymerized assembly of the aldonamide as helical coiled bilayer and tightly coiled to a tubule (*bottom*). Reproduced in part with permission from [212]

realized [212]. These structures were covalently stabilized by (incomplete) topotactic polymerization of the ordered diacetylenic units forming polydiacetylene networks throughout the tube [210, 212]. Higher degrees of crosslinking and thus higher tubular stabilities were achieved with phosphatidylcholines by incorporating additional polymerizable vinyl or methacrylate groups at the chain ends [213]. All these stabilization approaches are restricted to solutions or suspensions, since crosslinking in the LC phase takes place in a highly intertubular fashion, yielding insoluble porous bulk material [206].

Fuhrhop and coworkers demonstrated the enhanced stability of tubular structures through the introduction of additional H-bonding-motifs into bolaamphiphiles [214]. Unsymmetric amphiphiles of hydrocarbon chains with amino and amino acid functionalities at the termini and amide functionalities within the chain, for instance in **81**, were shown to form suspensions in water consisting of open-ended tubular vesicles of monolayered membranes with an inner diameter of 50 nm and micrometer lengths. Unsaturated glycolipids of the type **79** were shown to assemble via a H-bonding array between sugar moieties,  $\pi, \pi$ -interactions between phenyl groups, and hydrophobic forces between hydrocarbon tails [215]. Upon cooling of hot aqueous solutions containing **79**, aggregation to tubular open-ended structures occurred giving inner diameters of 10–15 nm, lengths up to 100  $\mu\text{m}$ , and a membrane thickness of 8–15 nm, corresponding to two to four lipid-interdigitated bilayers. The formation of multilamellar tube-like structures using either diacetylenic phospholipids [216] or complexes of filamentous actin with cationic lipids in the form of ammonium salts [217] has also been reported.

Huge tubular structures have been achieved by the introduction of di- and triblock copolymers serving as amphiphiles [185, 218]. The introduction of single-backbone rod-coil copolymers allowed for microphase separation, and subsequent controlled crosslinking of the resulting ordered two or three dimensional oligomer assemblies, such as “2D polymers” [219], anisotropic mushrooms [220], nanofibers [221], and ribbons [222] was reported by Stupp and coworkers. Related two-dimensional polymers based on crosslinked sheets of self-assembled ionic amphiphiles were described by Kunitake et al. [223].

Diblock copolymer amphiphiles such as polystyrene-*block*-poly(ethyleneoxide) [224] or poly(ethyleneoxide)-*block*-poly(ethylene) [225] were observed to form tubular bilayer aggregates in solution under appropriate conditions. Compared to small molecule assemblies, these systems display increased thermal stabilities but possess closed termini resembling cylindrical micelles. Additional stabilization by internal crosslinking of similar poly(butadiene)-*block*-poly(ethyleneoxide) copolymers forming worm-like micelles in solution was reported by Bates and his group [226]. However, the structure generated was not hollow.

A sophisticated approach towards hollow, open-ended tubes was reported by Stewart and Liu (Fig. 48) [227]. Polymers **83** composed of polyisoprene, poly(2-cinnamoyl ethyl methacrylate) (PCMA), and poly(*tert*-butyl acrylate) (PtBA)

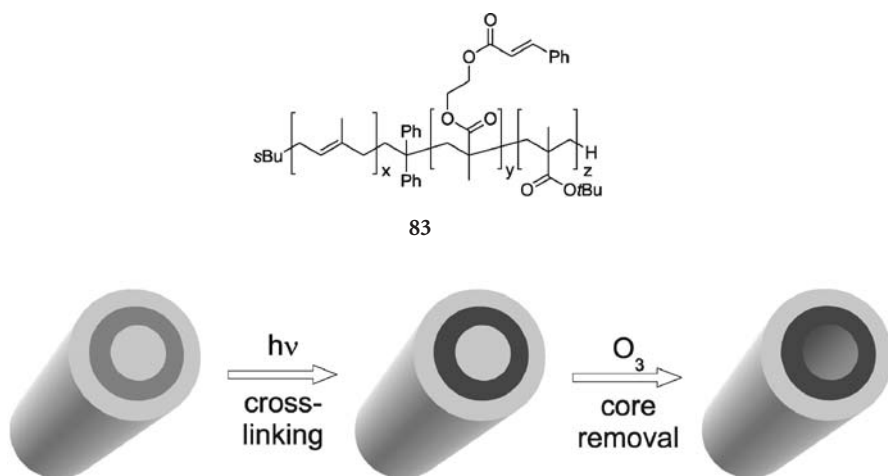


**Fig. 48** Stewart's and Liu's approach to polymeric nanotubes based on block copolymer assembly followed by photocrosslinking of the poly(2-cinnamoyl ethyl methacrylate) (PCMA) shell and removal of the polyisoprene core by ozonolysis

blocks were demonstrated to form cylindrical micelles in solution. The ratio of the blocks determines the size and shape of the assemblies. Ratios of approximately 1:1:6 (130:130:800 repeating units) lead to cylindrical micelles having dimensions of 79 nm in diameter and a few micrometers in length with a wide length distribution. Polyisoprene formed the core surrounded by a PCMA shell and a *Pt*BA corona. Photocrosslinking of the methacrylate shell was performed up to a conversion of 50% under retention of the cylindrical structure while the *Pt*BA prevented intertubular crosslinking. Subsequent removal of the polyisoprene core by ozonolysis, referred to by the authors as “nanosculpturing”, afforded a hollow polyacrylate tube that could be filled with guests demonstrating the opened termini.

Very recently, the assembly of amphiphilic hyperbranched multi-arm copolymers into stable and soluble tubes was reported [228]. Apparently, only a certain fraction of the polydisperse and ill-defined amphiphiles aggregates to multi-walled tubes of centimeter lengths and millimeter diameters visible to the naked eye.

## 8 Conclusions and Outlook

The tremendous progress that has been made in the research area outlined above has been sparked and guided by many recent advances in both covalent and non-covalent syntheses. On the one hand, the preparation of many new oligomer series necessary to deduce structure–property relationships has been

facilitated by rapid-growth approaches and the use of polymeric supports and reagents/catalysts. On the other hand, supramolecular science has evolved and grasped a much deeper understanding of the fundamental principles of self-assembly. The advent of dynamic covalent chemistry taking advantage of both areas and combining them with combinatorial methodology exemplifies perhaps the most powerful recent development. Last but not least, the availability of sophisticated analytical tools, most notably scanning probe techniques, has had a significant impact on the chemical sciences in general.

However, past accomplishments cannot eclipse the many related problems that await their solutions. Besides the general quest to further develop the above-mentioned disciplines, specific future challenges related to the development of functional organic nanotubes include:

1. Creating hollow tubes by developing strategies to overcome attractive van der Waals forces, and create tubes with an exploitable interior that can be tuned by means of postfunctionalization.
2. Increasing the aspect ratio by developing helical backbones that can be prepared in a living polymerization process and generating multi-stranded polymeric helices with an inner void.
3. Controlling the growth in a self-assembly process by incorporating subtle structural distortions or utilizing templates in order to achieve length control.
4. Stabilizing individual nanotubes by developing suitable crosslinking reactions that involve negligible geometrical changes but provide significantly enhanced robustness.
5. Integrating the tubular nanoobjects by incorporating them into larger hierarchical structures and connecting them to solid substrate surfaces.
6. Developing beneficial applications in nanofabrication, smart materials, and biotechnology.

The last point seems to be of particular importance, since a continuously dynamic development of the field will only occur if advantageous properties of the nanotubes are revealed and emerging technological applications provide the necessary driving force. Hopefully, this review has – at least to some extent – risen to the expectations of the expert and – perhaps more importantly – generated interest in entering and contributing to this fascinating field at the interface of chemistry, physics, and biology.

**Acknowledgments** Generous support by the Sofja Kovalevskaja Award of the Alexander von Humboldt Foundation, endowed by the Federal Ministry of Education and Research (BMBF) within the Program for Investment in the Future (ZIP) of the German Government, is gratefully acknowledged. MABB thanks the Studienstiftung des Deutschen Volkes for providing a doctoral fellowship.

## References

1. For a recent comment on Moore's law, see: Marsh G (2003) *Mater Today* 6:28
2. Special Issue "Nanotechnology" (2001) *Sci Am* 285:32
3. Love JC, Whitesides GM (2001) *Sci Am* 285:39
4. Lehn J-M (1995) *Supramolecular chemistry: concepts and perspectives*. VCH, Weinheim
5. Hecht S (2003) *Angew Chem Int Ed* 42:24
6. For rod-like modules, see: Schwab PFH, Levin MD, Michl J (1999) *Chem Rev* 99:1863
7. Special Issue "Supramolecular Chemistry & Self-Assembly" (2002) *Science* 295:2395 (and references therein)
8. For example: Yazdani A, Lieber CM (1999) *Nature* 401:227
9. For an excellent and inspiring review, consult: Bong DT, Clark TD, Granja JR, Ghadiri MR (2001) *Angew Chem Int Ed* 40:988
10. Clark CGJ, Wooley KL (2001) Regioselectively-crosslinked nanostructures. In: Fréchet JM, Tomalia DA (eds) *Dendrimers and other Dendritic Polymers*. Wiley, p 148
11. Special Issue "Carbon Nanotubes" (2001) *Top Appl Phys* 80:1
12. Special Issue "Carbon Nanotubes" (2002) *Acc Chem Res* 35:997
13. Xia Y, Yang P, Sun Y, Wu Y, Mayers B, Gates B, Yin Y, Kim F, Yan H (2003) *Adv Mater* 15:353
14. Steinhart M, Wendorff JH, Greiner A, Wehrspohn RB, Nielsch K, Schilling J, Choi J, Gösele U (2002) *Science* 296:1997
15. Bognitzki M, Hou H, Ishaque M, Frese T, Hellwig M, Schwarte C, Schaper A, Wendorff JH, Greiner A (2000) *Adv Mater* 12:637
16. Collins PG, Avouris P (2000) *Sci Am* 283:62
17. Hirsch A (2002) *Angew Chem Int Ed* 41:1853
18. See also chapter 5 of this volume
19. Sattler M, Liang H, Nettesheim D, Meadows RP, Harlan JE, Eberstadt M, Yoon HS, Shuker SB, Chang BS, Minn AJ, Thompson CB, Fesik SW (1997) *Science* 275:983
20. Ketchum RR, Hu W, Cross TA (1993) *Science* 261:1457
21. Jackson DS, Grant ME (1974) *Nature* 249:406
22. McDermott G, Prince SM, Freer AA, Hawthornthwaite-Lawless AM, Papiz MZ, Cogdell RJ, Isaacs NW (1995) *Nature* 374:517
23. Nakano T, Okamoto Y (2001) *Chem Rev* 101:4013
24. Hill DJ, Mio MJ, Prince RB, Hughes TS, Moore JS (2001) *Chem Rev* 101:3893
25. Urbano A (2003) *Angew Chem Int Ed* 42:3986
26. Meurer KP, Voegtle F (1985) *Top Curr Chem* 127:1
27. Here, we define the inner cavity by the *empty* space within a tubular structure. The inner diameter has been calculated from X-ray crystallographic or modeling data by measuring the distance between opposing atoms at the inner rim, correcting for the helical pitch, and subtracting the corresponding van der Waals radii
28. Han S, Bond AD, Disch RL, Holmes D, Schulman JM, Teat SJ, Vollhardt KPC, Whitener GD (2002) *Angew Chem Int Ed* 41:3223
29. Han S, Anderson DR, Bond AD, Chu HV, Disch RL, Holmes D, Schulman JM, Teat SJ, Vollhardt KPC, Whitener GD (2002) *Angew Chem Int Ed* 41:3227
30. De Santis P, Morosetti S, Rizzo R (1974) *Macromolecules* 7:52
31. Huc I (2004) *Eur J Org Chem* 1:17
32. Hamuro Y, Geib SJ, Hamilton AD (1994) *Angew Chem Int Ed Engl* 33:446
33. Hamuro Y, Geib SJ, Hamilton AD (1996) *J Am Chem Soc* 118:7529
34. Hamuro Y, Geib SJ, Hamilton AD (1997) *J Am Chem Soc* 119:10587
35. Zhu J, Parra RD, Zeng H, Skrzypczak-Jankun E, Zeng XC, Gong B (2000) *J Am Chem Soc* 122:4219

36. Gong B, Zeng H, Zhu J, Yuan L, Han Y, Cheng S, Furukawa M, Parra RD, Kovalevsky AY, Mills JL, Skrzypczak-Jankun E, Martinovic S, Smith RD, Zheng C, Szyperski T, Zeng XC (2002) *Proc Natl Acad Sci* 99:11583
37. Gong B (2001) *Chem Eur J* 7:4336
38. Cary JM, Moore JS (2002) *Org Lett* 4:4663
39. Yang X, Brown AL, Furukawa M, Li S, Gardinier WE, Bukowski EJ, Bright FV, Zheng C, Zeng XC, Gong B (2003) *Chem Commun* 56
40. Berl V, Huc I, Khoury RG, Krische MJ, Lehn J-M (2000) *Nature* 407:720
41. Berl V, Huc I, Khoury RG, Lehn J-M (2001) *Chem Eur J* 7:2798
42. Berl V, Huc I, Khoury RG, Lehn J-M (2001) *Chem Eur J* 7:2810
43. Dolain C, Maurizot V, Huc I (2003) *Angew Chem Int Ed* 42:2738
44. Kolomiets E, Berl V, Odriozola I, Stadler A-M, Kyritsakas N, Lehn J-M (2003) *Chem Commun* 2868
45. Jiang H, Leger J-M, Huc I (2003) *J Am Chem Soc* 125:3448
46. Berl V, Krische MJ, Huc I, Lehn J-M, Schmutz M (2000) *Chem Eur J* 6:1938
47. van Gorp JJ, Vekemans JAJM, Meijer EW (2004) *Chem Commun* 60
48. Hanan GS, Lehn J-M, Kyritsakas N, Fischer J (1995) *J Chem Soc, Chem Commun* 765
49. Hanan GS, Schubert US, Volkmer D, Riviere E, Lehn J-M, Kyritsakas N, Fischer J (1997) *Can J Chem* 75:169
50. Bassani DM, Lehn J-M (1997) *Bull Soc Chim Fr* 134:897
51. Bassani DM, Lehn J-M, Baum G, Fenske D (1997) *Angew Chem Int Ed Engl* 36:1845
52. Ohkita M, Lehn J-M, Baum G, Fenske D (1999) *Chem Eur J* 5:3471
53. Barboiu M, Lehn J-M (2002) *Proc Natl Acad Sci* 99:5201
54. Barboiu M, Vaughan G, Kyritsakas N, Lehn J-M (2003) *Chem Eur J* 9:763
55. Gardinier KM, Khoury RG, Lehn J-M (2000) *Chem Eur J* 6:4124
56. Schmitt J-L, Stadler A-M, Kyritsakas N, Lehn J-M (2003) *Helv Chim Acta* 86:1598
57. Cuccia LA, Lehn J-M, Homo J-C, Schmutz M (2000) *Angew Chem Int Ed* 39:233
58. Petitjean A, Cuccia LA, Lehn J-M, Nierengarten H, Schmutz M (2002) *Angew Chem Int Ed* 41:1195
59. Nelson JC, Saven JG, Moore JS, Wolynes PG (1997) *Science* 277:1793
60. Matsuda K, Stone MT, Moore JS (2002) *J Am Chem Soc* 124:11836
61. Hunter CA, Lawson KR, Perkins J, Urch CJ (2001) *J Chem Soc Perkin Trans* 2:651
62. Meyer EA, Castellano RK, Diederich F (2003) *Angew Chem Int Ed* 42:1210
63. Lahiri S, Thompson JL, Moore JS (2000) *J Am Chem Soc* 122:11315
64. Brunsveld L, Prince RB, Meijer EW, Moore JS (2000) *Org Lett* 2:1525
65. Hill DJ, Moore JS (2002) *Proc Natl Acad Sci* 99:5053
66. Prince RB, Saven JG, Wolynes PG, Moore JS (1999) *J Am Chem Soc* 121:3114
67. Zimm BH, Bragg JK (1959) *J Chem Phys* 31:526
68. Gin MS, Yokozawa T, Prince RB, Moore JS (1999) *J Am Chem Soc* 121:2643
69. Gin MS, Moore JS (2000) *Org Lett* 2:135
70. Prince RB, Brunsveld L, Meijer EW, Moore JS (2000) *Angew Chem Int Ed* 39:228
71. Prince RB, Moore JS, Brunsveld L, Meijer EW (2001) *Chem Eur J* 7:4150
72. Prince RB, Okada T, Moore JS (1999) *Angew Chem Int Ed* 38:233
73. Prince RB, Barnes SA, Moore JS (2000) *J Am Chem Soc* 122:2758
74. Tanatani A, Mio MJ, Moore JS (2001) *J Am Chem Soc* 123:1792
75. Tanatani A, Hughes TS, Moore JS (2002) *Angew Chem Int Ed* 41:325
76. Rowan SJ, Cantrill SJ, Cousins GRL, Sanders JKM, Stoddart JF (2002) *Angew Chem Int Ed* 41:899
77. Nishinaga T, Tanatani A, Oh K, Moore JS (2002) *J Am Chem Soc* 124:5934
78. Zhao D, Moore JS (2003) *Org Biomol Chem* 1:3471
79. Oh K, Jeong K-S, Moore JS (2001) *Nature* 414:889

80. Oh K, Jeong K-S, Moore JS (2003) *J Org Chem* 68:8397
81. Zhao D, Moore JS (2003) *Macromolecules* 36:2712
82. Zhao D, Moore JS (2003) *J Am Chem Soc* 125:16294
83. Wooley KL (2000) *J Polym Sci, Part A: Polym Chem* 38:1397
84. Blackwell HE, Grubbs RH (1998) *Angew Chem Int Ed* 37:3281
85. Blackwell HE, Sadowsky JD, Howard RJ, Sampson JN, Chao JA, Steinmetz WE, O'Leary DJ, Grubbs RH (2001) *J Org Chem* 66:5291
86. Kumita JR, Smart OS, Woolley GA (2000) *Proc Natl Acad Sci* 97:3803
87. Flint DG, Kumita JR, Smart OS, Woolley GA (2002) *Chem Biol* 9:391
88. Hecht S, Khan A (2003) *Angew Chem Int Ed* 42:6021
89. Khan A, Hecht S (2004) *Chem Commun* 300
90. Cornelissen JJLM, Rowan AE, Nolte RJM, Sommerdijk NAJM (2001) *Chem Rev* 101:4039
91. Langs DA (1988) *Science* 241:188
92. Piguet C, Bernardinelli G, Hopfgartner G (1997) *Chem Rev* 97:2005
93. Williams A (1997) *Chem Eur J* 3:15
94. Albrecht M (2001) *Chem Rev* 101:3457
95. Prest P-J, Prince RB, Moore JS (1999) *J Am Chem Soc* 121:5933
96. Mio MJ, Prince RB, Moore JS, Kübel C, Martin DC (2000) *J Am Chem Soc* 122:6134
97. Kübel C, Mio MJ, Moore JS, Martin DC (2002) *J Am Chem Soc* 124:8605
98. Presnell SR, Cohen FE (1989) *Proc Natl Acad Sci* 86:6592
99. Doyle DA, Morais Cabral J, Pfuetzner RA, Kuo A, Gulbis JM, Cohen SL, Chait BT, MacKinnon R (1998) *Science* 280:69
100. Schafmeister CE, Miercke LJW, Stroud RM (1993) *Science* 262:734
101. Wyman TB, Nicol F, Zelphati O, Scaria PV, Plank C, Szoka FC Jr (1997) *Biochemistry* 36:3008
102. Matile S (2001) *Chem Soc Rev* 30:158
103. Flower DR (1996) *Biochem J* 318:1
104. Nagano N, Hutchinson EG, Thornton JM (1999) *Protein Sci* 8:2072
105. Song L, Hobaugh MR, Shustak C, Cheley S, Bayley H, Gouaux JE (1996) *Science* 274:1859
106. Sakai N, Matile S (2003) *Chem Commun* 2514
107. Baumeister B, Sakai N, Matile S (2000) *Angew Chem Int Ed* 39:1955
108. Das G, Talukdar P, Matile S (2002) *Science* 298:1600
109. Höger S (1999) *J Polym Sci, Part A: Polym Chem* 37:2685
110. Zhao D, Moore JS (2003) *Chem Commun* 807
111. Grave C, Schlüter AD (2002) *Eur J Org Chem* 3075
112. Ghadiri MR, Granja JR, Milligan RA, McRee DE, Khazanovich N (1993) *Nature* 366:324
113. Hartgerink JD, Clark TD, Ghadiri MR (1998) *Chem Eur J* 4:1367
114. Granja JR, Ghadiri MR (1994) *J Am Chem Soc* 116:10785
115. Khazanovich N, Granja JR, McRee DE, Milligan RA, Ghadiri MR (1994) *J Am Chem Soc* 116:6011
116. Ghadiri MR, Granja JR, Buehler LK (1994) *Nature* 369:301
117. Horne WS, Stout CD, Ghadiri MR (2003) *J Am Chem Soc* 125:9372
118. Seebach D, Matthews JL, Meden A, Wessels T, Baerlocher C, McCusker LB (1997) *Helv Chim Acta* 80:173
119. Clark TD, Buehler LK, Ghadiri MR (1998) *J Am Chem Soc* 120:651
120. Clark TD, Buriak JM, Kobayashi K, Isler MP, McRee DE, Ghadiri MR (1998) *J Am Chem Soc* 120:8949
121. Ranganathan D, Samant MP, Karle IL (2001) *J Am Chem Soc* 123:5619
122. Ranganathan D, Haridas V, Gilardi R, Karle IL (1998) *J Am Chem Soc* 120:10793
123. Gauthier D, Baillargeon P, Drouin M, Dory YL (2001) *Angew Chem Int Ed* 40:4635
124. Ranganathan D (2001) *Acc Chem Res* 34:919

125. Ashton PR, Brown CL, Menzer S, Nepogodiev SA, Stoddart JF, Williams DJ (1996) *Chem Eur J* 2:580
126. Ashton PR, Cantrill SJ, Gattuso G, Menzer S, Nepogodiev SA, Shipway AN, Stoddart JF, Williams DJ (1997) *Chem Eur J* 3:1299
127. Gattuso G, Menzer S, Nepogodiev SA, Stoddart JF, Williams DJ (1997) *Angew Chem Int Ed Engl* 36:1451
128. Grave C, Lentz D, Schäfer A, Samori P, Rabe JP, Franke P, Schlüter AD (2003) *J Am Chem Soc* 125:6907
129. Müller P, Uson I, Hensel V, Schlüter AD, Sheldrick GM (2001) *Helv Chim Acta* 84:778
130. Young JK, Moore JS (1995) In: Stang PJ, Diederich F (eds) *Modern Acetylene Chemistry*. VCH, Weinheim, Germany, p 415
131. Moore JS (1997) *Acc Chem Res* 30:402
132. Venkataraman D, Lee S, Zhang J, Moore JS (1994) *Nature* 371:591
133. Ge P-H, Fu W, Herrmann WA, Herdtweck E, Campana C, Adams RD, Bunz UHF (2000) *Angew Chem Int Ed* 39:3607
134. Hosokawa Y, Kawase T, Oda M (2001) *Chem Commun* 1948
135. Höger S, Morryson DL, Enkelmann V (2002) *J Am Chem Soc* 124:6734
136. Mindyuk OY, Stetzer MR, Gidalevitz D, Heiney PA, Nelson JC, Moore JS (1999) *Langmuir* 15:6897
137. Rapaport H, Kim HS, Kjaer K, Howes PB, Cohen S, Als-Nielsen J, Ghadiri MR, Leiserowitz L, Lahav M (1999) *J Am Chem Soc* 121:1186
138. Zhang J, Moore JS (1994) *J Am Chem Soc* 116:2655
139. Mindyuk O, Stetzer MR, Heiney PA, Nelson JC, Moore JS (1998) *Adv Mater* 10:1363
140. Leclair S, Baillargeon P, Skouta R, Gauthier D, Zhao Y, Dory YL (2004) *Angew Chem Int Ed* 43:349
141. Zhang J, Moore JS (1992) *J Am Chem Soc* 114:9701
142. Hunter CA, Sanders JKM (1990) *J Am Chem Soc* 112:5525
143. Prince RB (2000) Phenylene ethynylene foldamers: cooperative conformational transition, twist sense bias, molecular recognition properties, and solid-state organization. PhD thesis, University of Illinois
144. Tobe Y, Utsumi N, Kawabata K, Nagano A, Adachi K, Araki S, Sonoda M, Hirose K, Naemura K (2002) *J Am Chem Soc* 124:5350
145. Tobe Y, Utsumi N, Nagano A, Naemura K (1998) *Angew Chem Int Ed* 37:1285
146. Tobe Y, Nagano A, Kawabata K, Sonoda M, Naemura K (2000) *Org Lett* 2:3265
147. Höger S, Bonrad K, Mourran A, Beginn U, Möller M (2001) *J Am Chem Soc* 123:5651
148. Rosselli S, Ramminger A-D, Wagner T, Silier B, Wiegand S, Haussler W, Lieser G, Scheumann V, Höger S (2001) *Angew Chem Int Ed* 40:3138
149. Harada A, Li J, Kamachi M (1992) *Nature* 356:325
150. Harada A, Li J, Kamachi M (1993) *Nature* 364:516
151. Liu Y, You C-C, Zhang H-Y, Kang S-Z, Zhu C-F, Wang C (2001) *Nano Lett* 1:613
152. Zimmerman SC, Wendland MS, Rakow NA, Zharov I, Suslick KS (2002) *Nature* 418:399
153. Wendland MS, Zimmerman SC (1999) *J Am Chem Soc* 121:1389
154. Kim Y, Mayer MF, Zimmerman SC (2003) *Angew Chem Int Ed* 42:1121
155. Clark TD, Ghadiri MR (1995) *J Am Chem Soc* 117:12364
156. Clark TD, Kobayashi K, Ghadiri MR (1999) *Chem Eur J* 5:782
157. Venkataraman D, Gardner GB, Lee S, Moore JS (1995) *J Am Chem Soc* 117:11600
158. Orr GW, Barbour LJ, Atwood JL (1999) *Science* 285:1049
159. Williamson JR (1994) *Annu Rev Biophys Biomol Struct* 23:703
160. Marlow AL, Mezzina E, Spada GP, Masiero S, Davis JT, Gottarelli G (1999) *J Org Chem* 64:5116

161. Forman SL, Fettinger JC, Pieraccini S, Gottarelli G, Davis JT (2000) *J Am Chem Soc* 122:4060
162. Mezzina E, Mariani P, Itri R, Masiero S, Pieraccini S, Spada GP, Spinozzi F, Davis JT, Gottarelli G (2001) *Chem Eur J* 7:388
163. Sessler JL, Sathiosatham M, Doerr K, Lynch V, Abboud KA (2000) *Angew Chem Int Ed* 39:1300
164. Giorgi T, Lena S, Mariani P, Cremonini MA, Masiero S, Pieraccini S, Rabe JP, Samori P, Spada GP, Gottarelli G (2003) *J Am Chem Soc* 125:14741
165. Bonazzi S, Capobianco M, De Morais MM, Garbesi A, Gottarelli G, Mariani P, Ponzi Bossi MG, Spada GP, Tondelli L (1991) *J Am Chem Soc* 113:5809
166. Sidorov V, Kotch FW, Davis JT, El-Kouedi M (2000) *Chem Commun* 2369
167. Tirumala S, Davis JT (1997) *J Am Chem Soc* 119:2769
168. Cai M, Marlow AL, Fettinger JC, Fabris D, Haverlock TJ, Moyer BA, Davis JT (2000) *Angew Chem Int Ed* 39:1283
169. Chaput JC, Switzer C (1999) *Proc Natl Acad Sci* 96:10614
170. Bonazzi S, De Morais MM, Gottarelli G, Mariani P, Spada GP (1993) *Angew Chem Int Ed Engl* 32:248
171. Ciuchi F, Di Nicola G, Franz H, Gottarelli G, Mariani P, Ponzi Bossi MG, Spada GP (1994) *J Am Chem Soc* 116:7064
172. Zimmerman SC, Duerr BF (1992) *J Org Chem* 57:2215
173. Kolotuchin SV, Zimmerman SC (1998) *J Am Chem Soc* 120:9092
174. Whitesides GM, Simanek EE, Mathias JP, Seto CT, Chin D, Mammen M, Gordon DM (1995) *Acc Chem Res* 28:37
175. Choi IS, Li X, Simanek EE, Akaba R, Whitesides GM (1999) *Chem Mater* 11:684
176. Klok H-A, Jolliffe KA, Schauer CL, Prins LJ, Spatz JP, Möller M, Timmerman P, Reinhoudt DN (1999) *J Am Chem Soc* 121:7154
177. Kimizuka N, Kawasaki T, Hirata K, Kunitake T (1995) *J Am Chem Soc* 117:6360
178. Fenniri H, Mathivanan P, Vidale KL, Sherman DM, Hallenga K, Wood KV, Stowell JG (2001) *J Am Chem Soc* 123:3854
179. Fenniri H, Deng B-L, Ribbe AE (2002) *J Am Chem Soc* 124:11064
180. Jonkheijm P, Miura A, Zdanowska M, Hoeben FJM, De Feyter S, Schenning APHJ, De Schryver FC, Meijer EW (2004) *Angew Chem Int Ed* 43:74
181. Yang J, Marendaz J-L, Geib SJ, Hamilton AD (1994) *Tetrahedron Lett* 35:3665
182. Israelachvili JN (1985) *Intermolecular and surface forces: with applications to colloidal and biological systems*. Academic, London
183. Klug A (1983) *Angew Chem Int Ed Engl* 22:565
184. Fuhrhop JH, Helfrich W (1993) *Chem Rev* 93:1565
185. Bates FS (1991) *Science* 251:898
186. Lee M, Cho B-K, Zin W-C (2001) *Chem Rev* 101:3869
187. Percec V, Ahn CH, Ungar G, Yeardley DJP, Moller M, Sheiko SS (1998) *Nature* 391:161
188. Percec V, Johansson G, Heck J, Ungar G, Batty SV (1993) *J Chem Soc Perkin Trans 1*: 1411
189. Percec V, Heck J, Tomazos D, Falkenberg F, Blackwell H, Ungar G (1993) *J Chem Soc Perkin Trans 1*:2799
190. Percec V, Johansson G, Ungar G, Zhou J (1996) *J Am Chem Soc* 118:9855
191. Hudson SD, Jung HT, Percec V, Cho WD, Johansson G, Ungar G, Balagurusamy VSK (1997) *Science* 278:449
192. Percec V, Heck JA, Tomazos D, Ungar G (1993) *J Chem Soc Perkin Trans 2*:2381
193. Percec V, Glodde M, Bera TK, Miura Y, Shiyonovskaya I, Singer KD, Balagurusamy VSK, Heiney PA, Schnell I, Rapp A, Spiess HW, Hudson SD, Duan H (2002) *Nature* 419: 384

194. Percec V, Ahn C-H, Cho W-D, Jamieson AM, Kim J, Leman T, Schmidt M, Gerle M, Möller M, Prokhorova SA, Sheiko SS, Cheng SZD, Zhang A, Ungar G, Yeardley DJP (1998) *J Am Chem Soc* 120:8619
195. Gin DL, Gu W, Pindzola BA, Zhou WJ (2001) *Acc Chem Res* 34:973
196. Zhou W, Gu W, Xu Y, Pecinovsky CS, Gin DL (2003) *Langmuir* 19:6346
197. Kim C, Lee SJ, Lee IH, Kim KT, Song HH, Jeon H-J (2003) *Chem Mater* 15:3638
198. Ringsdorf H, Schlarb B, Venzmer J (1988) *Angew Chem Int Ed Engl* 28:113
199. Mueller A, O'Brien DF (2002) *Chem Rev* 102:727
200. Schnur JM (1993) *Science* 262:1669
201. Wilson-Kubalek EM, Brown RE, Celia H, Milligan RA (1998) *Proc Natl Acad Sci* 95:8040
202. Fuhrhop JH, Fritsch D (1986) *Acc Chem Res* 19:130
203. Imae T, Takahashi Y, Muramatsu H (1992) *J Am Chem Soc* 114:3414
204. Itojima Y, Ogawa Y, Tsuno K, Handa N, Yanagawa H (1992) *Biochemistry* 31:4757
205. Nakashima N, Asakuma S, Kunitake T (1985) *J Am Chem Soc* 107:509
206. Srisiri W, Sisson TM, O'Brien DE, McGrath KM, Han Y, Gruner SM (1997) *J Am Chem Soc* 119:4866
207. Georger JH, Singh A, Price RR, Schnur JM, Yager P, Schoen PE (1987) *J Am Chem Soc* 109:6169
208. Giuliani F, Guillod F, Greiner J, Krafft M-P, Riess JG (1996) *Chem Eur J* 2:1335
209. Fuhrhop J-H, Schnieder P, Boekema E, Helfrich W (1988) *J Am Chem Soc* 110:2861
210. Frankel DA, O'Brien DF (1994) *J Am Chem Soc* 116:10057
211. Fuhrhop JH, Blumtritt P, Lehmann C, Luger P (1991) *J Am Chem Soc* 113:7437
212. Frankel DA, O'Brien DF (1991) *J Am Chem Soc* 113:7436
213. Singh A, Markowitz MA (1994) *New J Chem* 18:377
214. Fuhrhop JH, Spiroski D, Boettcher C (1993) *J Am Chem Soc* 115:1600
215. John G, Jung JH, Minamikawa H, Yoshida K, Shimizu T (2002) *Chem Eur J* 8:5494
216. Thomas BN, Safinya CR, Plano RJ, Clark NA (1995) *Science* 267:1635
217. Wong GCL, Tang JX, Lin A, Li Y, Janmey PA, Safinya CR (2000) *Science* 288:2035
218. Antonietti M, Förster S (2003) *Adv Mater* 15:1323
219. Stupp SI, Son S, Lin HC, Li LS (1993) *Science* 259:59
220. Zubarev ER, Pralle MU, Li L, Stupp SI (1999) *Science* 283:523
221. Hartgerink JD, Beniash E, Stupp SI (2001) *Science* 294:1684
222. Sone ED, Zubarev ER, Stupp SI (2002) *Angew Chem Int Ed* 41:1705
223. Asakuma S, Okada H, Kunitake T (1991) *J Am Chem Soc* 113:1749
224. Yu K, Eisenberg A (1998) *Macromolecules* 31:3509
225. Discher BM, Won Y-Y, Ege DS, Lee JCM, Bates FS, Discher DE, Hammer DA (1999) *Science* 284:1143
226. Won Y-Y, Davis HT, Bates FS (1999) *Science* 283:960
227. Stewart S, Liu G (2000) *Angew Chem Int Ed* 39:340
228. Yan D, Zhou Y, Hou J (2004) *Science* 303:65